ALMA MATER STUDIORUM - UNIVERSITA DI BOLOGNA

SCUOLA DI INGEGNERIA E ARCHITETTURA

DIPARTIMENTO DI
INGEGNERIA DELL'ENERGIA ELETTRICA E DELL'INFORMAZIONE
"GUGLIELMO MARCONI"

INGEGNERIA ELETTRONICA

TESI DI LAUREA MAGISTRALE

in

SOLID STATE PHYSICAL CHEMISTRY

QUANTUM MECHANICAL STUDY AND MODELING OF MOLECULAR ELECTRONIC DEVICES

CANDIDATO:
ATA BANIAHMAD

RELATORE:
Chiar.mo Prof. RENATO COLLE
CORRELATORE:
Chiar.mo Prof. MASSIMO RUDAN

Anno Accademico 2015/16
Sessione III

Abstract

Molecular electronics pursues the use of molecules as fundamental electronic components. The inherent properties of molecules such as nano-size, low cost, scalability, and self-assembly are seen by many as a perfect complement to conventional silicon electronics. Molecule based electronics has captured the attention of a broad cross section of the scientific community.
Molecular electronics science includes the design of molecules with the desired functionality, the measurement of the electronic and structural properties of molecules, and the integration of molecules into operational devices. In molecular electronic devices, the possibility of having channels that are just one atomic layer thick, is perhaps the most attractive feature that takes the attention to graphene. Single-layer graphene is a purely two-dimensional material. Its lattice consists of regular hexagons with a carbon atom at each corner.The most advantage of graphene is its high carrier mobility at room temperature. The conductivity, stability, uniformity, composition, and 2D nature of graphene make it an excellent material for electronic devices.

In this thesis we focused on Zigzag Graphene NanoRibbon(ZGNR) as a transmission channel. Due to the importance of an accurate description of the quantum effects in the operation of graphene devices, a full-quantum transport model has been adopted: the electron dynamics has been described by Density Functional Theory(DFT) and transport has been solved within the formalism of Non-Equilibrium Green's Functions (NEGF). Using DFT and NEGF methods, the transport properties of ZGNR and ZGNR doped with Si are studied by systematically computing the transmission spectrum. It is observed that Si barrier destroyed the electronic transport properties of ZGNR, an energy gap appeared for ZGNR, and variations from conductor to semiconductor are displayed.
Its followed by a ZGNR grown on a SiO_2 crystal substrate, while substituting the Graphene electrodes with the Gold ones, and its effect on transmission properties have been studied. Improvement in transmission properties observed due to the formation of C-O bonds between ZGNR and substrate that make the ZGNR corrugated. Finally, we modeled a nano-scale Field Effect Transistor by implementing a gate under SiO_2 substrate. A very good I_{ON}/I_{OFF} ratio has been observed although the device thickness.
The atomic scale electronic devices, computationally implemented and used to best properties and efficiency of similar devices, make evidence the importance of using quantum mechanical models and computational methods to propose and test new molecular electronic devices.

Acknowledgment

It is my greatest pleasure to thank Professor Renato Colle who helped me bring this thesis to the light. I was incredibly fortunate to be able to work with and learn from him. I came to realize what a great scientist, a great teacher, and a great person he is. His constant pursuit of new ideas and uncompromising attention to important details imprinted in my mind a model of a great scientist. I cannot thank him enough for his trust and guidance academically and personally throughout my graduate study.

In addition, I would like to thank Professor Massimo Rudan, for his valuable guidance and providing what needed to choose the right direction.

Finally, my deep and sincere gratitude to my family for their continuous and unparalleled love, help and support.

Contents

Introduction

Molecular electronics can be traced back to the early 1970s, but it is only in the past decade that important experimental and theoretical hurdles have finally been overcome. Experiments with single-molecule junctions, have become more robust, reliable and reproducible. At the same time, theoretical methods based on Green's function theory have been developed and have allowed researchers to investigate the fundamental properties of single molecules under nonequilibrium conditions. These advances have led to the discovery of a host of novel effects that have only recently been systematically investigated. Concurrently, a variety of potential practical applications, which extend beyond the electronic devices predicted in the early days of the field, have also been proposed.
Molecules can do so much more and we are only at the beginning to understand their possibilities.

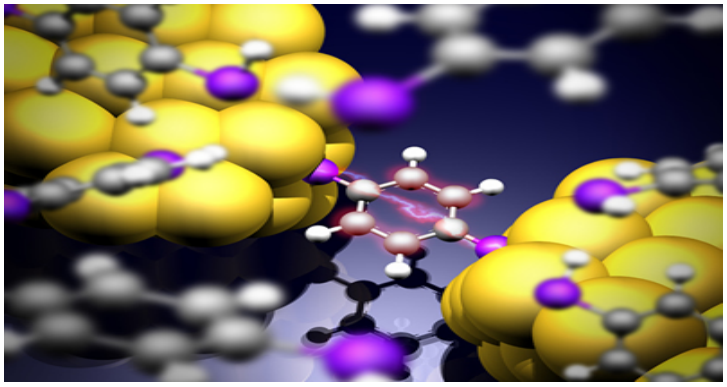

Figure: Schematic diagram of a single molecule bridging two metal electrodes, cover illustration of Physical Chemistry Chemical Physics(PCCP) journal.[1]

Molecular Electronics

Since around 1960, the minimum feature size of electronic components has decreased every two years by a factor of two. Alternatively, the number of components in an integrated circuit has doubled every two years. This observation is known as Moore's Law. It is expected that miniaturization of electronic components will reach a fundamental limit and Moore's Law will not longer be obeyed.

Molecular Electronics was proposed in 1974 as a possible technology capable of solving the miniaturization problem to extend Moore's Law. The main concept of Molecular Electronics is the use of a single molecule as individual electronic component in circuitry.

In 1974, Aviram devoted to the topic of a single molecule junction as a device, and as a model problem. Following the Aviram contribution, there was extensive interest in the general area of molecular electronics, but the difficulty of unambiguously creating the structure such as a single molecule bonded to two macroscopic electrodes was formidable.
The entire field changed with the invention of scanning probe microscopy in the early 1980s. First the scanning tunneling microscope(STM)[2] and then the atomic force microscope (AFM)[3] made it possible to apply a voltage across a single molecule, and to measure the current. In the 1980s and 1990s, several attempts were made to measure current through single molecules between two electrodes.
Within the next decade, the theory involved in modeling molecular transport, starting from the Landauer approach, and extending that to deal with strongly non-equilibrium situations using the Non Equilibrium Green's Function (NEGF) methodology permitted a straightforward recipe for expressing the flow of charge in terms of Green's functions and self-energies, which in turn could be calculated from electronic structure calculations.

A self-consistent scheme using a combination of Kohn-Sham Density Functional Theory (KS-DFT) and NEGF has become standard for modeling single molecule transport.

Molecular Functionality

The target of Molecular Electronics is to arrive at functional molecular components. Integrated circuits are based on a number of functional components such as transistors and diodes.

The original Aviram and Ratner unipolar rectification is based on an asymmetry of orbitals over a single molecule. It assumes perfect symmetric coupling to the metallic electrodes. The rectification is solely based on the molecule. Rectification, however, has been observed for a number of molecular electronic junctions. Asymmetric coupling with the electrodes, in energy and space, is responsible for rectification. The rectification ratio can be tuned. Symmetric molecules inside an asymmetric junction can then also

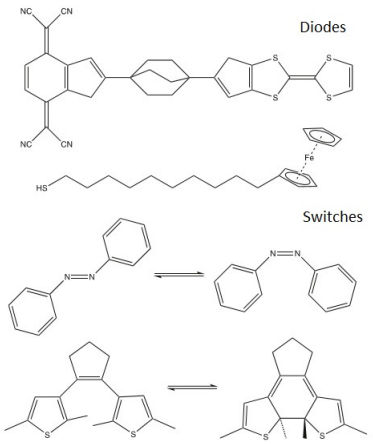

Figure 1: *Molecules that have been investigated for the realization of functional molecular junctions. The original Aviram and Ratner molecule*[4] *and a ferrocene compound used by Whitesides*[5] *are depicted as examples of diodes. As examples of resistive switches azobenzene and diarylethene photochromic cores are shown*[6].

lead to rectification.

A field-effect transistor is based on the modulation of the charge carrier density in a semiconductor channel between source and drain electrodes by an electric gate field. The channel of a transistor is positioned at the interface of a semiconductor and an insulator. By capacitive coupling of a third electrode with the semiconductor over the insulator, the amount of charge carriers in the channel is modulated. For adequate transistor performance, the thickness of the insulator should be around half of the channel length, i.e. half the size of the molecule of which the channel consists. Therefore, the incorporation of a gate dielectric in a single molecule has been theoretically investigated. The transistor then consists of a single molecule covalently bound to three electrodes.

Single molecule based logic is investigated. Several switching mechanisms within a single molecule are proposed. Multi-terminal molecules have been devised to act as complete logic gates such as AND or NOR gates. Although theoretically attractive and well described, experimental verification of the mechanisms for molecular based logic has not been reported.

For memory applications, two-terminal molecular diodes exhibiting bistable switching have been investigated. A broad range of organic compounds has been synthesized. The compounds exhibit two or more stable states which can be interchanged by external stimuli. The states can differ by electronic energy levels or conformation. External stimuli that can be used to interchange the states can be light, voltage or heat. Different types of molecular switches have been incorporated in molecular junctions. Voltage-based switching in junctions has been reported. The geometry of the molecular junctions is of importance. Molecules can loose switching properties by the fabrication of the electrical contacts to the molecules or the lack of conformational freedom.
Molecules might accomplish other functionalities as well. A resonant tunneling diode that exhibits negative differential resistance (NDR) has been reported.

In summary, molecules can perform a multitude of different functions in molecular junctions. The performance depends on the molecular structure, the electronic coupling to the electrode and the geometry of the molecular junction. Chemical synthesis can deliver many compounds and even yield molecules with completely unexpected and new functionalities.

In This Thesis

In this thesis, we focused on Zigzag Graphene NanoRibbon(ZGNR) as a transmission channel. Due to the importance of an accurate description of the quantum effects in the operation of Graphene devices, a full-quantum transport model has been adopted: the electron dynamics has been described by Density Functional Theory(DFT) and transport has been solved within the formalism of Non-Equilibrium Green's Functions(NEGF).

–In the 1^{st} chapter, we briefly summarize DFT going through Hohenberg-Kohn theorem and Kohn-Sham equations. Then we discuss approximation for exchange correlation functions, such as Local Density Approximation(LDA) and Generalized Gradient Approximation(GGA).

–In the 2^{nd} chapter, we summarize NEGF theory and discuss how it is going to be used in computing density matrix and current probability.

–In the 3^{rd} chapter, we discuss about modeling the electronic transport in single-channel mesoscopic conductor.

–In the 4^{th} chapter, we summarize mathematics behind Atomistix Toolkit(ATK) simulator software, as it is so much important for us to know exactly what simulation software is doing behind and how it gains its results.

In the next 3 chapters, we start to model a nano scale systems, and study their electronic transport properties, by computing transmission spectrum, current spectrum, transmission pathways and I(V) curve.

–In the 5^{th} chapter, we worked on Graphene NanoRibbon between graphene electrodes and studied how silicon barrier affect transmission properties of Graphene NanoRibbon.

–In the 6^{th} chapter, we considered devices with electrodes made of materials different from that of the conductor. We used gold electrodes, and grown Graphene NanoRibbon on SiO_2 substrate for the channel and compare their results with those obtained with Graphene NanoRibbon between Graphene electrodes.

–In the last chapter, we modeled and studied the nano scale Field Effect Transistor with channel made of graphene grown on silicon dioxide.

Chapter 1

1 Density Functional Theory

Density Functional Theory (DFT) is a ground-state theory in which the emphasis is on the charge density as the relevant physical quantity. DFT has proved to be highly successful in describing structural and electronic properties in a vast class of materials, ranging from atoms and molecules to simple crystals to complex extended systems (including glasses and liquids). Furthermore DFT is computationally simple. For these reasons DFT has become a common tool in first-principles calculations aimed at describing or even predicting properties of molecular and condensed matter systems.

1.1 The Hohenberg-Kohn Theorem

Let us consider a system of N interacting (spinless) electrons under an external potential V(r) (usually the Coulomb potential of the nuclei). If the system has a nondegenerate ground state, it is obvious that there is only one ground-state charge density n(r) that corresponds to a given V(r). In 1964 Hohenberg and Kohn demonstrated the opposite, far less obvious result: there is only one external potential V(r) that yields a given ground state charge density n(r). The demonstration is very simple.

Let us consider a many-electron Hamiltonian H = T + U + V, with ground state wave function Ψ. T is the kinetic energy, U the electron-electron interaction potential, V the external potential. The charge density n(r) is defined as

$$n(r) = N \int |\Psi(r, r_2, r_3, ..., r_N)|^2 dr_2 ... dr_N \tag{1}$$

Let us consider now a different Hamiltonian H'= T + U + V' (V and V' do not differ simply by a constant: V-$V'\neq$ const.), with ground state wave function Ψ'. Let us assume that the ground state charge densities are the same: n[V]=$n'[V']$. The following inequality holds:

$$E' = \langle \Psi' \mid H' \mid \Psi' \rangle < \langle \Psi \mid H' \mid \Psi \rangle = \langle \Psi \mid H + V' - V \mid \Psi \rangle \tag{2}$$

that is,

$$E' < E + \int [V(r) - V'(r)] n(r) dr \tag{3}$$

The inequality is strict because Ψ and Ψ' are different, being eigenstates of different Hamiltonians. By reversing the primed and unprimed quantities, one obtains an absurd result. This demonstrates that no two different potentials can have the same charge density. A subtle point about the existence of the potential corresponding to a given ground state charge density (the v-representability problem), and the various extensions of the Hohenberg and Kohn theorem, are discussed in the specialized literature. A straightforward consequence of the first Hohenberg and Kohn theorem is that the ground state energy E is also uniquely determined by the ground-state charge density. In mathematical terms E is a functional E[n(r)] of n(r). We can write

$$E[n(r)] = \langle \Psi \mid T + U + V \mid \Psi \rangle = \langle \Psi \mid T + U \mid \Psi \rangle + \langle \Psi \mid V \mid \Psi \rangle = F[n(r)] + \int n(r)V(r)dr \tag{4}$$

where E[n(r)] is a universal functional of the charge density n(r) (and not of V (r)). For this functional a variational principle holds: the ground-state energy is minimized by the ground-state charge density. In this way, DFT exactly reduces the N-body problem to the determination of a 3-dimensional function n(r) which minimizes a functional E[n(r)]. Unfortunately this is of little use as E[n(r)] is not known.

1.2 The Kohn-Sham equations

One year later, Kohn and Sham (KS) reformulated the problem in a more familiar form and opened the way to practical applications of DFT. The system of interacting electrons is mapped on to an auxiliary system of non-interacting electrons having the same ground state charge density n(r). For a system of non-interacting electrons the ground-state charge density is representable as a sum over one-electron orbitals (the KS orbitals) $\psi_i(r)$:

$$n(r) = 2\sum_i \mid \psi_i(r) \mid^2 \tag{5}$$

where i runs from 1 to N/2 if we assume double occupancy of all states, and the KS orbitals are the solutions of the Schrodinger equation

$$(-\frac{\hbar^2}{2m}\nabla^2 + V_{KS}(r))\psi_i(r) = \epsilon_i\psi_i(r) \tag{6}$$

(m is the electron mass) obeying orthonormality constraints:

$$\int \psi_i^*(r)\psi_j(r)dr = \delta_{ij} \tag{7}$$

The existence of a unique potential $V_{KS}(r)$ having n(r) as its ground state charge density is a consequence of the Hohenberg and Kohn theorem, which holds irrespective of the form of the electron-electron interaction U.

The problem is now to determine $V_{KS}(r)$ for a given n(r). This problem is solved by considering the variational property of the energy. For an arbitrary variation of the $\psi_i(r)$, under the orthonormality constraints of Eq.(7), the variation of E must vanish. This translates into the condition that the functional derivative with respect to the ψ_i of the constrained functional

$$E' = E - \sum_{ij} \lambda_{ij} [\int \psi_i^*(r)\psi_j(r)dr - \delta_{ij}] \tag{8}$$

where δ_{ij} are Lagrange multipliers, must vanish:

$$\frac{\delta E'}{\delta \psi_i^*(r)} = \frac{\delta E'}{\delta \psi_i(r)} = 0 \tag{9}$$

It is convenient to rewrite the energy functional as follows:

$$E = T_s([n(r)] + E_H[n(r)] + E_{xc}[n(r)] + \int n(r)V(r)dr \tag{10}$$

The first term is the kinetic energy of non-interacting electrons:

$$T_s[n(r)] = -\frac{\hbar^2}{2m} 2 \sum_i \int \psi_i^*(r)\nabla^2\psi_i(r)dr \tag{11}$$

The second term (called the Hartree energy) contains the electrostatic interactions between clouds of charge:

$$E_H[n(r)] = \frac{e^2}{2} \int \frac{n(r)n(r')}{\mid r - r' \mid} dr dr' \tag{12}$$

The third term, called the exchange-correlation energy, contains all the remaining terms: our ignorance is hidden there. The logic behind such procedure is to subtract out easily computable terms which account for a large fraction of the total energy. Using

$$\frac{\delta_n(r)}{\delta \psi_i^*(r)} = \psi_i(r)\delta(r - r') \tag{13}$$

we find

$$\frac{\delta T_s}{\delta \psi_i^*(r)} = -\frac{\hbar^2}{2m} 2 \sum_i \nabla^2\psi_i(r) \tag{14}$$

$$\frac{\delta E_H}{\delta \psi_i^*(r)} = e^2 \int \frac{n(r')}{\mid r - r' \mid} dr' \psi_i(r) \tag{15}$$

and finally

$$(-\frac{\hbar^2}{2m}\nabla^2 + V_H(r) + V_{xc}[n(r)] + V(r))\psi_i(r) = \sum_j \lambda_{ij}\psi_j(r) \tag{16}$$

where we have introduced a Hartree potential

$$V_H(r) = e^2 \int \frac{n(r')}{\mid r - r' \mid} dr \tag{17}$$

and an exchange-correlation potential

$$V_{xc}[n(r)] = \frac{\delta E_{xc}}{\delta n(r)} \tag{18}$$

The Lagrange multiplier λ_{ij} are obtained by multiplying both sides of Eq.16 by $\psi_k^*(r)$ and integrating:

$$\lambda_{ik} = \int \psi_k^*(r)(-\frac{\hbar^2}{2m}\nabla^2 + V_H(r) + V_{xc}[n(r)] + V(r))\psi_i(r)dr \tag{19}$$

For an insulator, whose 1-electron states are either fully occupied or completely empty, it is always possible to make a subspace rotation in the space of ψ's (leaving the charge density invariant). We finally get the KS equations:

$$(H_{KS} - E_i)\psi_i(r) = 0 \tag{20}$$

where $\lambda_{ij} = \delta_{ij}\epsilon_j$ and the operator H_{KS}, called KS Hamiltonian, is defined as

$$H_{KS} = (-\frac{\hbar^2}{2m}\nabla^2 + V_H(r) + V_{xc}(r) + V(r) = -\frac{\hbar^2}{2m}\nabla^2 + V_{KS}(r) \tag{21}$$

and is related to the functional derivative of the energy:

$$\frac{\delta E}{\delta \psi_i^*(r)} = H_{KS}\psi_i(r) \tag{22}$$

1.3 The local density approximation (LDA)

The local density approximation (LDA) is the basis of all approximate exchange-correlation functionals. At the center of this model is the idea of an uniform electron gas. This is a system in which electrons move on a positive background charge distribution such that the total ensemble is neutral. The central idea of LDA is the assumption that we can write E_{XC} in the following form

$$E_{XC}^{LDA}[\rho] = \int \rho(\overrightarrow{r}) E_{xc}[\rho(\overrightarrow{r})] d\overrightarrow{r} \tag{23}$$

Here,$E_{xc}[\rho(\overrightarrow{r})]$ is the exchange-correlation energy per particle of an uniform electron gas of density $\rho(\overrightarrow{r})$. This energy per particle is weighted with the probability $\rho(\overrightarrow{r})$ that there is an electron at this position. The quantity $E_{xc}[\rho(\overrightarrow{r})]$ can be further split into exchange and correlation contributions,

$$E_{xc}[\rho(\overrightarrow{r})] = E_x[\rho(\overrightarrow{r})] + E_c[\rho(\overrightarrow{r})] \tag{24}$$

The exchange part, E_x, which represents the exchange energy of an electron in a uniform electron gas of a particular density, was originally derived by Bloch and Dirac in the late 1920's

$$E_x = -\frac{3}{4}[\frac{3\rho(\overrightarrow{r})}{\pi}]^{\frac{1}{3}} \tag{25}$$

No such explicit expression is known for the correlation part, E_c. However, highly accurate numerical quantum Monte-Carlo simulations of the homogeneous electron gas are available (Ceperly-Alder, 1980).
The accuracy of the LDA for the exchange energy is typically within 10 %,while the normally much smaller correlation energy is generally overestimated by up to a factor 2. The two errors typically cancel partially.
This moderate accuracy that LDA delivers is certainly insufficient for most applications in chemistry.
LDA can also fail in systems, like heavy Fermions, so dominated by electron-electron interaction effects.

1.4 The generalized gradient approximation (GGA)

The first logical step to go beyond LDA is the use of not only the information about the density $\rho(\overrightarrow{r})$ at a particular point $\overrightarrow{r}$, but to supplement the density with information about the gradient of the charge density, $\nabla\rho(\overrightarrow{r})$ in order to account for the non-homogeneity of the true electron density.

Thus, we write the exchange correlation energy in the following form termed generalized gradient approximation(GGA),

$$E_{xc}^{GGA}[\rho_\alpha, \rho_\beta] = \int f[\rho_\alpha, \rho_\beta, \nabla\rho_\alpha, \nabla\rho_\beta] d\overrightarrow{r} \tag{26}$$

Thanks to much thoughtful work, important progress has been made in deriving successful GGA's. Their construction has made use of sum rules, general scaling properties.
Using a definition approach Becke introduced a successful hybrid functional:

$$E_{xc}^{hyb} = \alpha E_x^{KS} + (1-\alpha) E_{xc}^{GGA} \tag{27}$$

where E_x^{KS} is the exchange calculated with the exact KS wave function, E_{xc}^{GGA} is an appropriate GGA, and α is a fitting parameter.
GGA's and hybrid approximations has reduced the LDA errors on atomization energies of standard set of small molecules by a factor 3-5. This improved accuracy has made DFT a significant component of quantum chemistry.
All the present functionals are inadequate for situations where the density is not a slowly varying function. Examples are (a) Wigner crystals; (b) electronic tails evanescencing into the vacuum near the surfaces of bounded electronic systems. However, this does not preclude that DFT with appropriate approximations can successfully deal with such problems.

Chapter 2

2 Non Equilibrium Green's Function

Non equilibrium Green's function(NEGF) is a general method for modeling non-equilibrium quantum transport in open mesoscopic systems with many body scattering effect.
Electron density matrix and current can be expressed easily in terms of Green's function in a simple form.
Using NEGF, transport and scattering transport have been studied.

2.1 Introduction

In principle, all interacting quantum many-body systems in equilibrium and non equilibrium are completely described by a sufficiently large set of N-particle wave functions $|\Psi_{N,i}\rangle \equiv \Psi_{N,i}(q_1...q_N, t)$ entering the time-dependent Schrodinger equation(TDSE) as $i\delta_t|\Psi_{N,i}\rangle = H(t)|\Psi_{N,i}\rangle$, where
$q_i \equiv x_i\delta_i$ are the space and spin variables of particle i. The associated Hamiltonian in coordinate representation thereby attains the form

$$H(t) = \sum_{i=1}^{N} h^0(x_i, t) + \sum_{i<j} w(x_i - x'_j) \quad , h^0(x_i, t) = -\frac{\hbar^2}{2m}\nabla^2_{x_i} + v(x_i, t) \quad (28)$$

where $h^0(x_i, t)$ denotes the one-particle contributions containing kinetic energy and a (generally time-dependent) potential $v(x_i, t)$. Further, $w(x_i - x_j)$ is a specific pair-interaction potential added up over all $N(N_1)/2$ classically distinguishable pairs (x_i, x_j) and, for simplicity, spin degrees of freedom have been neglected.
The wave function $|\Psi_{N,i}\rangle$ has to fulfill the correct symmetry, i.e. must be (anti)symmetric under particle exchange for bosons of zero or integer spin (fermions of odd half-integer spin). While it is simple to construct exact (anti-) symmetric wave functions in few-particle systems ($N \leq 3$), this becomes an intricate task for larger N, and in general one has to call on group theoretical considerations. Moreover, it is not trivial to incorporate thermodynamic situations where the interacting many-body system is connected to a given bath of finite temperature $k_BT = \beta^{-1}$ and, therefore, requires a respective statistical treatment.
Thus, apart from first principle approaches based on microscopic footings, it is more fruitful to proceed with a quantum field theoretical description. Using the second quantization language such a method equally applies to Fermi

and Bose systems and, in particular, allows one to overcome the problem of (anti-)symmetrizing the wave functions as symmetry properties and spin statistics are automatically included and preserved. Furthermore, in combination with quantum statistics, ensemble averages become available at finite temperatures, which offers a profound basis to establish the (non)equilibrium Green's functions.

2.2 Green's functions

Time-independent Schrodinger equation:

$$H \mid n\rangle = E \mid n\rangle \tag{29}$$

We divide the Hamiltonian and wavefunction of the system into contact $(H_{1,2}, |\psi_{1,2}\rangle)$ and device $(H_d, |\psi_d\rangle)$ subspaces:

$$\begin{pmatrix} H_1 & \tau_1 & o \\ \tau_1^\dagger & H_d & \tau_2^\dagger \\ 0 & \tau_2 & H_2 \end{pmatrix} \begin{pmatrix} \mid \psi_1\rangle \\ \mid \psi_d\rangle \\ \mid \psi_2\rangle \end{pmatrix} = E \begin{pmatrix} \mid \psi_1\rangle \\ \mid \psi_d\rangle \\ \mid \psi_2\rangle \end{pmatrix}$$

where $\tau_{1,2}$ describes the interaction between device and contacts. In general we have N contacts $(H_1, ..., n)$ connecting $(\tau_1, ..., n)$ the device H_d to the reservoirs. Here we will assume that the contacts are independent, i.e., there are no cross terms (τ) between the different contacts. We define the Green's function $G(E)$ by means of the equation:

$$(E - H)G(E) = I \tag{30}$$

The Green's function gives the response of a system to a constant perturbation $|v\rangle$ in the Schrodinger equation:

$$H \mid \psi\rangle = E \mid \psi\rangle + \mid v\rangle \tag{31}$$

The response to this perturbation is:

$$(E - H) \mid \psi\rangle = - \mid v\rangle \tag{32}$$

$$\mid \psi\rangle = -G(E) \mid v\rangle \tag{33}$$

The reason of needing the response to this type of perturbation is that it's usually easier to calculate the Green's function than solve the whole eigenvalue problems and most (all for the one-particle system) properties of the system can be calculated from the Green's function.

For example, the wavefunction of the contact ($|\Psi_i\rangle$) can be calculated if we know the wavefunction on the device ($|\Psi_d\rangle$).
The reason for calculating the Green's function is that it is easier than solving the Schrodinger equation.
Non equilibrium Green's function methods are regularly used to calculate current and charge densities in nanoscale (both molecular and semiconductor) conductors under bias. This method is mainly used for ballistic conduction, but may be extended to include inelastic scattering. In the following we explain the NEGF equations for the current and charge density matrix.

2.3 Charge density matrix

In the non-equilibrium case, we are often interested in two quantities: the current and the charge density matrix. Lets start with the charge density (which allows us to use a self-consistent scheme to describe charging). The charge density matrix is defined as:

$$\rho = \sum_k f(k,\mu) \mid \psi_k\rangle\langle\psi_k \mid \tag{34}$$

where the sum runs over all states with occupation number $f(E_k,\mu)$ (pure density matrix). The occupation number is determined by the reservoirs filling the incoming waves in the contacts such that:

$$f(E_k,\mu_1) = \frac{1}{1+e^{(E_k-\mu_1)/K_BT}} \tag{35}$$

is the Fermi-Dirac function with chemical potential(μ_1) and temperature(T) of the reservoir responsible for injecting electrons into the contacts.
The wavefunction of the device represented by an incoming wave is:

$$\mid \psi_{d,k}\rangle = G_d\tau_1^\dagger \mid \psi_{1,k}\rangle \tag{36}$$

Adding up all states gives:

$$\rho_d = \int_{E=-\infty}^{\infty} dE \sum_k f(E,\mu_1)\delta(E-E_k) \mid \psi_d,k\rangle\langle\psi_d,k \mid \tag{37}$$

$$= \int_{E=-\infty}^{\infty} dE f(E,\mu_1) \sum_k \delta(E-E_k) G_d\tau_1^\dagger \mid \psi_1,k\rangle\langle\psi_1,k \mid \tau_1 G_d^\dagger \tag{38}$$

$$= \int_{E=-\infty}^{\infty} dE f(E,\mu_1) G_d\tau_1^\dagger [\sum_k \delta(E-E_k) \mid \psi_1,k\rangle\langle\psi_1,k \mid] \tau_1 G_d^\dagger \tag{39}$$

$$= \int_{E=-\infty}^{\infty} dEf(E,\mu_1)G_d\tau_1^\dagger \frac{a_1(E)}{2\pi}\tau_1 G_d^\dagger \quad , a_1(E) = \sum_k \delta(E-E_k) \mid \psi_1,k\rangle\langle\psi_1,k \mid \tag{40}$$

Defining the new quantity $\Gamma_1 = \tau_1^\dagger a_1 \tau_1$ we obtain the final expression for the charge density of the device:

$$\rho_\alpha = \frac{1}{2\pi}\int_{E=-\infty}^{\infty} dEf(E,\mu_1)G_d\Gamma_1 G_d^\dagger \tag{41}$$

The total charge density thus becomes a sum over all contacts:

$$\rho = \frac{2(forspin)}{2\pi}\int_{E=-\infty}^{\infty} dE\sum_i f(E,\mu_i)G_d\Gamma_i G_d^\dagger \tag{42}$$

2.4 Probability Current

Having different chemical potentials in the reservoirs filling the contacts gives rise to a current. In the next section we will calculate this current in a similar way as the charge density was calculated. But to do this we need an expression for the current from the wave function. In the continuum case we can calculate the current from the velocity operator. However, for a discrete Hamiltonian it is not so clear what the velocity operator is. Therefore, we derive an expression for the current from the continuity equation (using two contacts). In steady-state, the probability to find an electron on the device($\sum_n \mid \Psi_n \mid^2$ where the sum runs over the device subspace) is conserved:

$$0 = \frac{\delta \sum_n \mid \psi_n \mid^2}{\delta t} = \sum_n \frac{\delta\langle\psi \mid n\rangle\langle n \mid \psi\rangle}{\delta t} = \sum_n [\frac{\delta\langle\psi \mid n\rangle}{\delta t}\langle n \mid \psi\rangle + \langle\psi \mid n\rangle\frac{\delta\langle n \mid \psi\rangle}{\delta t}] \tag{43}$$

$$= \frac{i}{\hbar}\sum_n [\langle\psi \mid H \mid n\rangle\langle n \mid \psi\rangle - \langle\psi \mid n\rangle\langle n \mid H \mid \psi\rangle] = \frac{i}{\hbar}[\langle\psi \mid H \mid \psi_d\rangle - \langle\psi_d \mid H \mid \psi\rangle] \tag{44}$$

Using $H = H_d + \tau_1 + \tau_2$, we obtain

$$0 = \frac{i}{\hbar}([\langle\psi_1 \mid \tau_1 \mid \psi_d\rangle - \langle\psi_d \mid \tau_1^\dagger \mid \psi_1\rangle] + [\langle\psi_2 \mid \tau_2 \mid \psi_d\rangle - \langle\psi_d \mid \tau_2^\dagger \mid \psi_2\rangle]) \tag{45}$$

We interpret the term in the first (square) bracket as the incoming probability current into the device from contact 1 and the second bracket from contact 2. Generalizing to an arbitrary contact j gives us the electron current (at a given energy) as the charge (-e) times the probability current:

$$i_j = -\frac{ie}{\hbar}[\langle \psi_j \mid \tau_j \mid \psi_d \rangle - \langle \psi_d \mid \tau_j^\dagger \mid \psi_j \rangle] \tag{46}$$

where i_j is defined as positive for a current from the contacts into the device.

2.5 Electron Current

To calculate the total electron current through the device, we only need to put in the wavefunctions of the device and contacts($\mid \psi_d\rangle, \mid \psi_1\rangle, \mid \psi_2\rangle$) and add all the contributions together. Thus the current flowing into the device from an incoming wave of energy (E) in contact 1 ($\mid \psi_{1,n}\rangle$) through the coupling defined by τ_2 is given by:

$$i_{2\to 1} = -\frac{ie}{\hbar}[\langle \psi_2 \mid \tau_2 \mid \tau_d \rangle - \langle \psi_d \mid \tau_2^\dagger \mid \psi_2 \rangle] \tag{47}$$

$$= \frac{e}{\hbar}\langle \psi_{1,n} \mid \tau_1 G_d^\dagger \Gamma_2 G_d \tau_1^\dagger \mid \psi_{1,n} \rangle \tag{48}$$

Adding over the modes (n) and noting that the levels are filled from the reservoir connected to contact 1 gives:

$$I_{2\to 1} = 2\frac{e}{\hbar}\int_{E=-\infty}^{\infty} dE f(E,\mu_1) \sum_n \delta(E-E_n)\langle \psi_{1,n} \mid \tau_1 G_d^\dagger \Gamma_2 G_d \tau_1^\dagger \mid \psi_{1,n} \rangle \tag{49}$$

$$= \frac{e}{\pi\hbar}\int_{E=-\infty}^{\infty} dE f(E,\mu_1) T_r(G_d^\dagger \Gamma_2 G_d \Gamma_1) \tag{50}$$

Where factor 2 is for spin.
To get the total current through the device, the current from contact two have to be subtracted away:

$$I = \frac{e}{\pi\hbar}\int_{E=-\infty}^{\infty} dE[f(E,\mu_1) - f(E,\mu_2)] T_r(G_d^\dagger \Gamma_2 G_d \Gamma_1) \tag{51}$$

which is exactly the Landauer formula for the current.

Chapter 3

3 Modeling the Electronic Transport in Single-Channel Mesoscopic Conductors

The electronic current flowing through a mesoscopic device(dimensions between ∼5 and 100 nm) at T∼ $0°k$ under the effect of an external applied potential, can be defined proportional to the probability that one electron of energy ϵ flows from electrode 1 (chemical potential = μ_1) to electrode 2 (μ_2) with $\mu_1 < \epsilon < \mu_2$.

It is clear that the standard definition of conductance: $G = \sigma\frac{W}{L}$, where σ depends on the channel material, cannot be applied for $L \to 0$, since experimental evidences show that G tends to a finite value in this limit.
This fact is usually attributed to the arising of resistances at the contacts between channel and electrodes, but it can be quantitatively predicted only using quantum mechanical models.
Let us utilize first the "Effective Mass Equation" for the dynamics of an electron in conduction band:

$$[\frac{|\ i\hbar\overrightarrow{\bigtriangledown} + e\overrightarrow{A}\ |^2}{2m_c} + V(\overrightarrow{r}) + \epsilon_c]\ \psi(\overrightarrow{r}) = \epsilon\ \psi(\overrightarrow{r}) \tag{52}$$

Where $\overrightarrow{A}$ is the vector potential, V an external potential (not that due to the atomic structure of the crystal), ϵ_c the bottom of the band, and $m_c = \hbar^2[\frac{\delta^2\epsilon_c(h)}{\delta k^2}]^{-1}_{k=k_0}$ is the effective mass, that takes into account effects due to the nuclear attraction potential.

Solution of the eigenvalue equation can be written in the form:

$$\psi_{n\,\overrightarrow{k}}(\bar{i}) = \phi_n(z)e^{ik_x.x}e^{ik_y.y}; \quad \epsilon_n(k) = \epsilon_c + (\frac{\hbar^2k^2}{2n}) + \epsilon_n \tag{53}$$

for an electron moving along z under a continual potential that produces sub bands numbered by the indexen. The $\pm k$ states are occupied by electrons moving respectively from the left(+k) and from the right(-k) electrode with occupation numbers respectively of $f_{+k} = f_0(\epsilon - \mu_1)$ and $f_{-k} = f_0(\epsilon - \mu_2)$, where $f(x)$ is the Fermi function.

The probability current associate to the +k state is $J_{+k} = \frac{\hbar k}{nL}$ and the

number of occupied sub-bands at ϵ_k is $M(\epsilon_k) = \sum_J \theta(\epsilon_k - \epsilon_J)$ where $\theta(x)$ is the step function for a balistic conductor (transmission probability=1). All the left incoming electrons will come out through the right electrode, and each bound gives the following contribution to the current:

$$I = 2(-q) \sum_k \frac{\hbar k}{nl} [f_0(\epsilon_k - \mu_L) - f_0(\epsilon_k - \mu_R)] \qquad (2 for spin) \qquad (54)$$

that in the limit of $\Delta\epsilon_{k,k+1} \to 0$ becomes

$$I = \frac{-2q}{\hbar} \int_0^{\epsilon_k} [f_0(\epsilon - \mu_L) - f_0(\epsilon - \mu_R)] \; M(\epsilon) d\epsilon$$

if $M(\epsilon) = M$, one has $I = -\frac{2q}{\hbar} M(\mu_L - \mu_R)$ and $G = \frac{2q^2}{\hbar} M$. Note that, for macroscopic conductors, one has $M \to \infty$ and the resistance $\to 0$, while for mesoscopic conductors the interface effects become important.

3.1 Many Channel Mesoscopic Conductor

We generalize here the previous 1-channel model to the case of a many-channel system in the energy range of interest for left and right electrodes: $\mu_R < E < \mu_L$.

To this end we define 4 types of currents:
$\overrightarrow{i_L}(E), \overleftarrow{i_R}(E)$ outgoing currents from L,R electrodes
$\overleftarrow{i_L}(E), \overrightarrow{i_R}(E)$ incoming currents to L,R electrodes
in terms of active modes $M_{L,R}$ and transmission probabilities $T_{L,R}$ from left and right electrodes

$$\overrightarrow{i_L}(E) = -\frac{2q}{\hbar} M_L f_L(E) \qquad \overleftarrow{i_L}(E) = T_R \overleftarrow{i_R} + (1 - T_L) \overrightarrow{i_L} \qquad (55)$$

$$\overleftarrow{i_R}(E) = -\frac{2q}{\hbar} M_R f_R(E) \qquad \overrightarrow{i_R}(E) = (1 - T_R) \overleftarrow{i_R} + T_L \overrightarrow{i_L} \qquad (56)$$

where $f_{L,R}(E)$ are Fermi functions for L,R electrodes.
The net current per energy, following in the circuit, is:

$$i(E) = \overrightarrow{i_L}(E) - \overleftarrow{i_L}(E) = -\frac{2q}{h} \; [\overline{T_L}(E) f_L(E) - \overline{T_R}(E) f_k(E)] \qquad (57)$$

where $\overline{T_{L,R}} = T_{L,R} M_{L,R}$ are the left, right transmission probabilities weighted by the numbers of active modes in the L,R electrodes.

The total current in the circuit is $I = \int i(E)dE$. Note that, when the system is at the equilibrium, one can assume $\overline{T_L} = \overline{T_R} = T(E)$ with

$$i(E) = -\frac{2q}{h}\, T(E)\, [f_L(E) - f_R(E)] \tag{58}$$

and

$$I = -\frac{2q}{h} \int T(E)[f_L(E) - f_R(E)]dE = -\frac{1}{q} \int G(E)dE \tag{59}$$

where the conductance function is defined as

$$G(E) = \frac{2q^2}{h} \int T(E')F_t(E' - E)dE'; \qquad F_t(E) = \frac{1}{4k_B t_k} sech^2(\frac{E}{k_B t_k}) \tag{60}$$

and F_t gives the thermal broadening.

Chapter 4

4 Mathematics behind Simulator

The procedure of studying electronic transport through a nano-scale system typically involves a mathematical model for the simulation of nano-scale systems, and the subsequent analysis of the data obtained from the simulation software. It is so important for us to know exactly what the simulation software is doing behind and how it gains its results.

In the next following chapter of this thesis, we are going to design an atomic scale quantum system and start to calculate its properties using Atomistix ToolKit(ATK)[13,14] as a simulation software especially designed for quantum systems. So we should know exactly what kind of calculations and mathematics are implemented in this software to have a better overview of the results we are going to gain.

ATK can model electronic properties of equilibrium and non equilibrium quantum systems respectively in the framework of the Kohn-Sham Density Functional Theory(KS-DFT), and of the Non-Equilibrium Green's Function(NEGF) method. The Key quantity used by the ATK code is the density matrix, where diagonal term, obtained via solution of the Kohn-Sham(KS) equations, defining the equilibrium electronic density. On the other hand, using the Non-Equilibrium Green's Function(NEGF) method, ATK calculates the Non-Equilibrium electron density for open systems.
The next section describes the computational methods implemented in the ATK codes.

4.1 KS-DFT

In this context, the electronic structure of isolated atomic, molecular and solid state systems can be obtained using the one-electron KS-Hamiltonian:

$$\widehat{F}_{KS} = -\frac{\hbar^2}{2m}\nabla^2 + V_{KS}[n](r) \tag{61}$$

Where the first term is the one electron kinetic energy operator, while the second term is an effective potential inside which electrons are moving under the electrostatic attractive potential of the ions and an effective repulsive potential due to the other electrons. The key quantity to represent the electronic systems is the density matrix $P_1(\overrightarrow{r_1}, \overrightarrow{r_2})$ where diagonal

part$P_1(\overrightarrow{r_1}, \overrightarrow{r_2}) = n(r)$ is the local electronic density. This quantity can be expressed in terms of the eigenfunctions of the one particle KS operator:

$$\widehat{F}_{KS} = \frac{p^2}{2m} + V_{eff}[n] \tag{62}$$

where the effective one particle potential that governs the electronic motion can be splitted as follows:

$$V_{eff}[n] = V_H[n] + V_{XC}[n] + V_{ext} \tag{63}$$

where V_H is the mean field repulsive potential due to the other electrons, V_{ext} is the coulomb attraction potential due to the molecular plus that due to other possible external fields and V_{XC} is the exchange correlation potential.

4.2 Solving the Kohn-Sham equations

To calculate the one-electron eigenfunctions $[\psi_\alpha^{KS}]$ of $\widehat{F}_{KS}$, we have to solve the following one-electron Schrodinger equation, at fixed molecular position (Bohr-Oppenheimer approximation):

$$\widehat{F}_{KS}\psi_\alpha(r) = \epsilon_\alpha \psi_\alpha(r) \tag{64}$$

A way to solve it is to expand the electronic eigenfunctions $[\psi_\alpha(r)]$ in a set of basis functions, $\{\phi_i\}$:

$$\psi_\alpha(r) = \sum_i C_{\alpha i}\phi_i(r) \tag{65}$$

This allows to represent the differential Eq.2 as a matrix equation whose solutions give the expansion coefficients, $\{C_{\alpha i}\}$

$$\sum_j H_{ij}C_{\alpha j} = \epsilon_\alpha \sum_j S_{ijC_{\alpha j}} \tag{66}$$

where $\{H_{ij} = \langle \phi_i \mid \widehat{H}_{1el} \mid \phi_j \rangle\}$, is the Hamiltonian matrix and $\{S_{ij} = \langle \phi_i \mid \phi_j \rangle\}$ is the overlap matrix between the basis functions.

4.3 Electron density

The electron density of the many-electron system is given by the occupied eigenstates of the Kohn-Sham Hamiltonian:

$$n(r) = \sum_\alpha \mid \psi_\alpha(r) \mid^2 f(\frac{\epsilon_\alpha - \epsilon_f}{KT}) \tag{67}$$

where $f(x) = 1/(1 + e^x)$ is the Fermi function, ϵ_F the Fermi energy, and T the electron temperature. The electron density can be represented in terms of the density matrix, $\{D_{ij}\}$:

$$n(r) = \sum_{ij} \phi_i(r) D_{ij} \phi_j(r) \tag{68}$$

where its elements can expressed in terms of the basis set expansion coefficients $C_{\alpha i}$ as follows:

$$D_{ij} = \sum_{\alpha} C^*_{\alpha i} C_{\alpha j} f(\frac{\epsilon_\alpha - \epsilon_f}{KT}) \tag{69}$$

4.4 Exchange-correlation functionals

In the DFT method, the quantum mechanical part of the electron-electron interaction is approximated by the exchange-correlation term,in which a large number of different approximate exchange-correlation density functionals have been proposed.What we use here, is the so-called Generalized-Gradient Approximation (GGA).
The GGA functionals are a large family of semi-local approximations for the exchange-correlation density energy, where the functional depends on both the local value and the local gradient of the electron density,

$$E^{GGA}[n] = \int n(r) \epsilon^{GGA}(n(r), \nabla n(r)) dr \tag{70}$$

4.5 NEGF formalism as implemented in ATK code

The device configuration consists of 3 regions: Left electrode(LE), Central region(CR), Right electrode(RE).

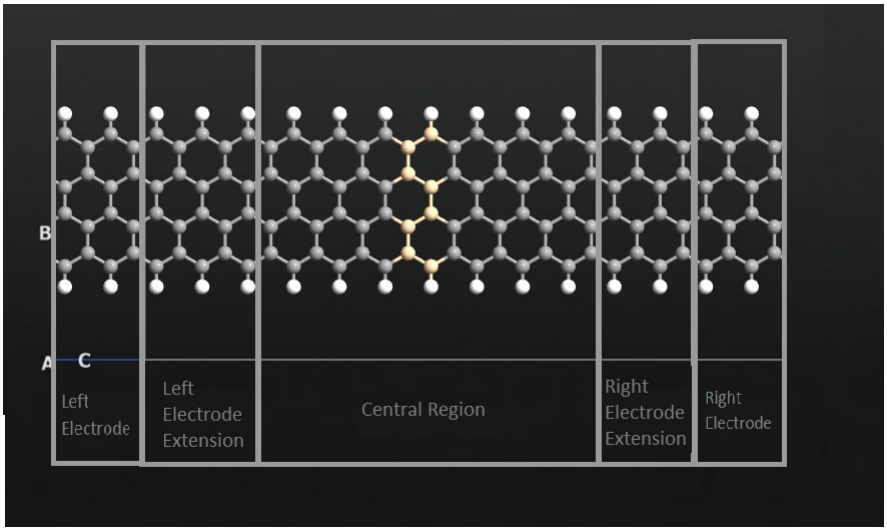

The implementation of the NEGF method is based on the Screening Approximation(SA) assuming that properties of Left and Right regions can be obtained from bulk calculations for the fully periodic electrode cell. SA is usually satisfied where the current through the system is sufficiently small to assume that the electrodes have equilibrium electron distribution. The key problem is the calculation of the non-equilibrium electron distribution in the central region.

The basic assumption is that the system is in a steady state such that the electron density $n(\overrightarrow{r})$ in the device central region is time-independent, and given by the sum of the required molecules of the occupied scattering states. Since the chemical potentials($\mu_{L/R}^{+/-}$) of the two electrodes are different for applied bias voltage: $\mu_R^- - \mu_L^+ = eV_b$. The contribution of each electrode to the total electron density in the central region has to be calculated independently, in terms of the occupied scattering states:

$$n(r) = n_L(r) + n_R(r) = \sum_{\alpha} \mid \psi_{\alpha}^{L}(r) \mid^2 f(\frac{\epsilon_{\alpha}^{L} - \mu_L}{KT}) + \sum_{\alpha} \mid \psi_{\alpha}^{R}(r) \mid^2 f(\frac{\epsilon_{\alpha}^{R} - \mu_R}{KT}) \tag{71}$$

The scattering states are obtained by first calculating the Bloch states in the crystal electrodes and then solving the Schrodinger Equation in the central region of the device, using the calculated Bloch states as Boundary Conditions.

Instead of using scattering states for calculating the non-equilibrium density, ATK uses the Non-Equilibrium Green's Function(NEGF) method, that can be summarized as follows:

The electron density is given in terms of the electron density matrix, $D = D_L + D_R$, having a left contribution(D_L) and a right contribution(D_R), both calculated using the NEGF method.[1]

The Left Density Matrix is calculated as

$$D_L = \int \rho_L(\epsilon) f(\frac{\epsilon - \mu_L}{KT_L}) d\epsilon \tag{72}$$

where

$$\rho_L(\epsilon) = \frac{1}{2\pi} G(\epsilon) \Gamma_L(\epsilon) G^\dagger(\epsilon) \tag{73}$$

is the Spectral Density Matrix.

We notice that the device central region has a non-equilibrium electron distribution, which the electron distribution in the electrode is given by a Fermi function at the temperature T_L of the left electrode.

Furthermore $G(\epsilon)$ is the Retarded Green's Function, and

$$\Gamma_L = -i[\Sigma_L(\epsilon) - \Sigma_L(\epsilon)^\dagger] \tag{74}$$

is the broadening function of the left electrode expressed in terms of the left electrode self energy: $\Sigma_L(\epsilon)$. Similar quantities have to be calculated for the right electrode. Note that the energy integral required to obtain the Density Matrices is evaluated through a complex contour interaction, divided in an integral over equilibrium states and another over non-equilibrium states.

4.5.1 Retarded Green's Function Matrix

$$G(\epsilon) = \lim_{\delta_+ \to 0} \frac{1}{(\epsilon + i\delta_+)S - H} \tag{75}$$

Where H and S are the Hamiltonian and overlap matrices of the entire system.
The calculation of $G(\epsilon)$ can be restricted to the central region using the following expression:

$$G(\epsilon) = [(\epsilon + i\delta_+)S - H - \Sigma^L(\epsilon) - \Sigma^L(\epsilon)]^{-1} \tag{76}$$

Where $\Sigma^{L,R}(\epsilon)$ are the self energies that describe the effects of the L and R electrodes on the electronic structure of the central region.

4.5.2 Effective Hamiltonian

V_{eff} is the sum of the exchange-correlation potential and of the electrostatic Hartee potential:

$$V_{eff}(r) = V_{XC}(r) + V_H(r) \tag{77}$$

It is a local or semi local function of the density, but $V_H(r)$ is defined up to an arbitrary constant. In particular, the Hartee potentials of the two electrodes are aligned through their chemical potential(Fermi levels) that are related by the applied bias(V_b).

$$\mu_R - \mu_L = eV_b \tag{78}$$

The Hartee potential of the central region is obtained by solving the Poisson's equation, using the bulk like Hartee potentials of the electrodes as boundary conditions at the interfaces between electrodes and central region.

4.5.3 Transmission Coefficient

It can be obtained from the Retarded Green's Function as follows:

$$T(\epsilon) = G(\epsilon)\Gamma^L(\epsilon)G^\dagger(\epsilon)\Gamma^R(\epsilon) \tag{79}$$

and it can be used to calculate the current and differential conductance.

4.5.4 Electrical Current

It can obtained from the transmission spectrum.

Chapter 5

5 How do Silicon Barrier affect transmission properties of Graphene NanoRibbon?

This chapter contains 2 different systems which are made of Graphene NanoRibbon. We start with a perfect Graphene NanoRibbon and continue with ribbon where Carbon atoms of Graphene have been substituted with Silicon atoms to work as a barrier. The geometry of each system has been optimized by minimizing the energy of the system. On each optimized geometry, I(V) curve, transmission spectra, current spectra and transmission pathway have been calculated and the results are going to be compared. Graphene electrodes have been used to reduce the computational time.

5.1 Graphene NanoRibbon

Relaxed structure of 2*2 Zig-Zag Graphene NanoRibbon with fundamental unit repeated 9 times along C direction is illustrated in Fig. 1.
The length of each electrode is $4.92^{\circ}A$ and 25% of central region considered as electrode extension part on each side and the whole structure relaxed via energy(E) minimization.

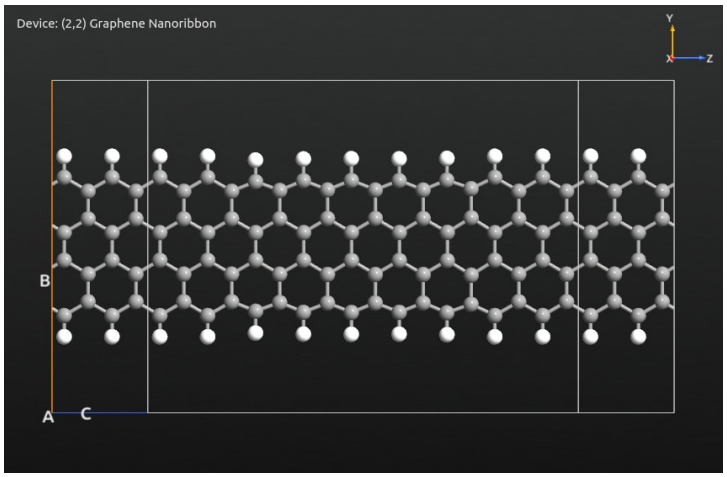

Figure 1: ZigZag Garphene NanoRibbon, Saturated by hydrogen atoms at the sides

The central region has been relaxed by minimizing the energy of the structure with respect to the geometrical parameters on this device. We calculated the following quantities defined in details in the previous chapters, see also [Ref. 13].
1) Electronic current:

$$I(V) = \frac{2e^2}{h} \int_{-\infty}^{+\infty} d\epsilon [n_F(\epsilon - \mu_L) - n_F(\epsilon - \mu_R)] * T_r[\Gamma^\dagger \Gamma(\epsilon)] \tag{80}$$

2) Derivative of the electronic current:

$$\frac{dI(V)}{dV} \tag{81}$$

3) Left to right transmission amplitude matrix:

$$t(\epsilon) = [\Gamma_R(\epsilon)]^{1/2} G(\epsilon) \ [\Gamma_L(\epsilon)]^{1/2} = U_R \ diag\{|\ \tau_n\ |\} U_L^\dagger \tag{82}$$

defined in terms of its eigenvalue and eigenvector.

5.1.1 I and dI/dV curves

The electronic current through the contacts: I(V), and its derivatives: dI/dV have been plotted, respectively in Fig 2a and 2b.
We can observe that I(V) is an antisymmetric function of the voltage: I(V)= -I(-V), while its derivative symmetric is: $\frac{dI}{dV}(V) = \frac{dI}{dV}(-V)$.

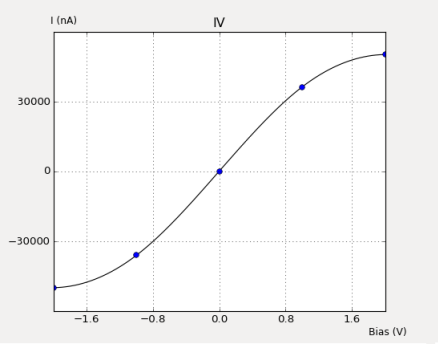

Figure 2a: I(V) curve of GNR

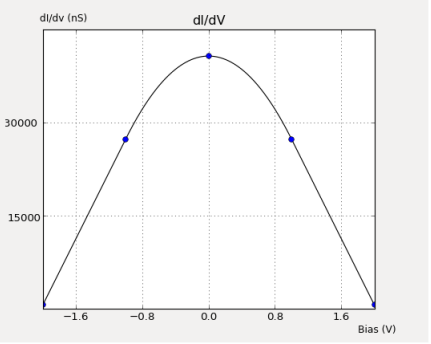

Figure 2b: dI/dV curve of GNR

5.1.2 Transmission Spectra

The total transmission spectrum $T(\epsilon) = \sum_n \mid \tau_n \mid^2$ is the sum of the eigenvalues of the transmission amplitude matrix [see Ref 13] and is plotted as function of the energy in Fig. 3a, b, c, respectively, for applied voltage: V= 0, +1, +2 volt(s). We notice step behavior of the plots at $V > 0$.

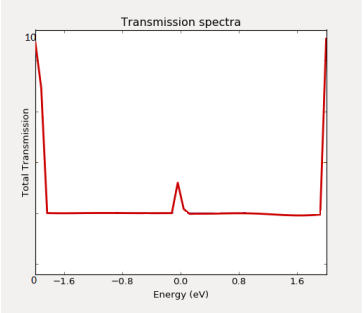

V=0

Figure 3a: Transmission Spectra as function of the energy

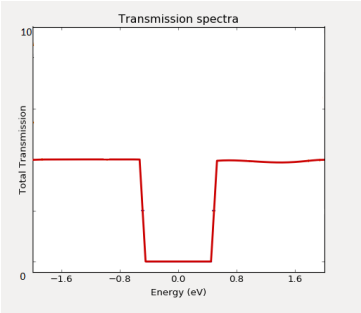

V=+1v

Figure 3b: Transmission Spectra decreases at $-0.4ev < \epsilon < 0.4ev$ by applying $V = +1v$

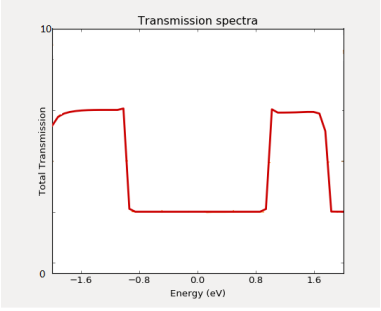

V=+2v

Figure 3c: Transmission Spectra decreases at $-0.8ev < \epsilon < 0.8ev$ by applying $V = +2v$

Note that $T(\epsilon, V) = T(\epsilon, -V)$ because of the device symmetry.

5.1.3 Spectral current

The spectral current defined as the integral over the Landauer formula [see Ref. 13] and is plotted in Fig. 4a, b, c for applied voltage: V= 0, +1, +2, volt(s), respectively.

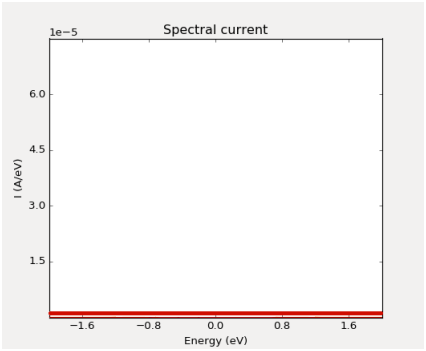

V=0

Figure 4a: No current spectral at V=0

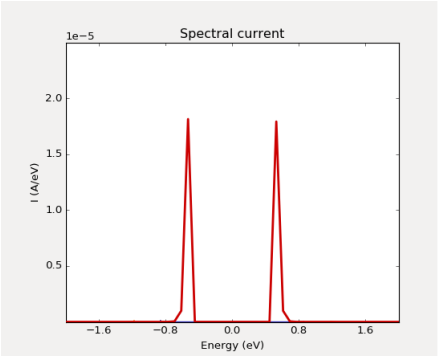

V=+1v

Figure 4b: Peaks at $\epsilon = +0.7ev$ and $-o.7ev$ at V=+1v

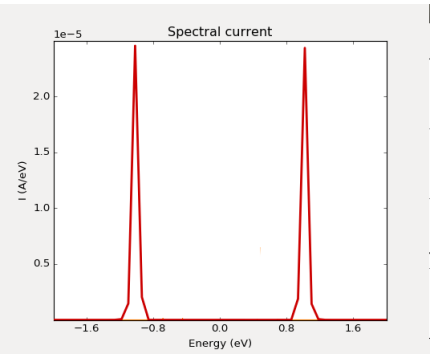

V=+2v

Figure 4c: Peaks at $\epsilon = +1.2ev$ and $-1.2ev$ at V=+2v

5.1.4 Transmission pathways

Transmission pathways shows how electrons propagate through device at a specific energy value.
Fig 6 shows transmission pathways through the device at $\epsilon = 0\, ev$, and $V = 0$. Preferred channels (red lines) are the shortest paths going through C-C bonds from left to right electrode. These channels are the eigenvectors of $\mid G\,\Gamma_L\,G^{\dagger}\,\Gamma_R \mid$ [see Ref 13]

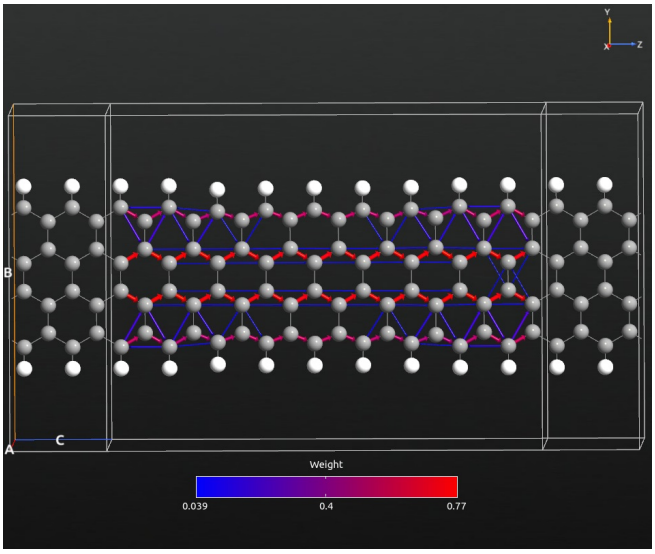

Fig 6: Transmission pathways at the Fermi level for the perfect Graphene NanoRibbon

5.2 Graphene NanoRibbon with Silicon barrier

Relaxed structure of 2*2 Graphene NanoRibbon with fundamental unit repeated 9 time along C direction and 6 C atoms substituted by 6 Si atoms that work as a barrier.
4.92 Angstrom is the length of each electrode with 25 percent of the central region at each side used as an electrode extension part.

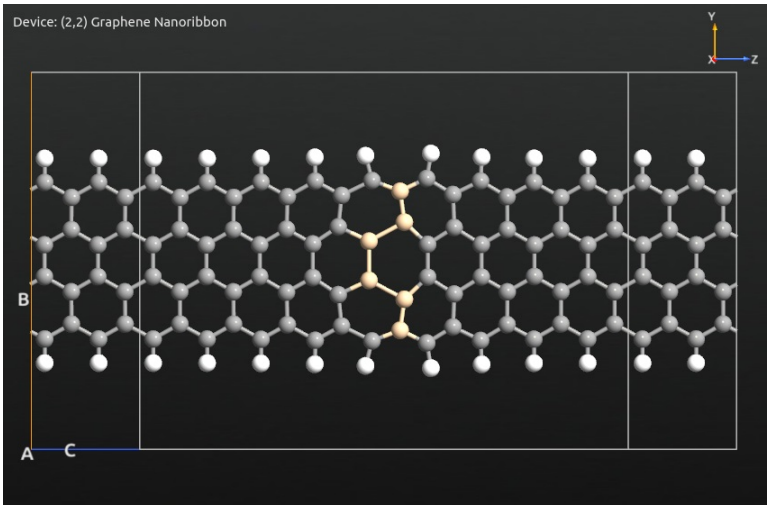

Figure 7: ZigZag Garphene NanoRibbon, Saturated at the sides, 6 Si atoms substituted to work as a barrier

5.2.1 I and dI/dV curves

The electronic current through the contacts; I(V), and its derivatives; dI/dV have been plotted as function of V, respectively in Fig 8a and 8b.

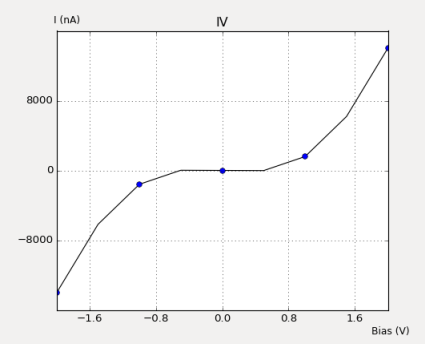

Figure 8a: I(V) curve of GNR with Si barrier

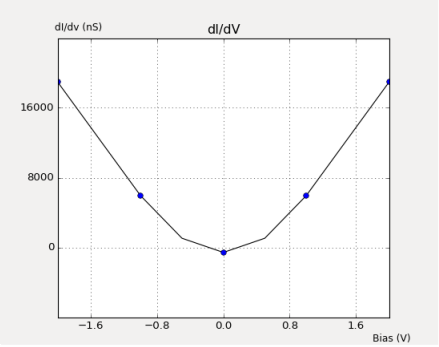

Figure 8b: dI/dV curve of GNR with Si barrier

We see that Si atoms act as a barrier between the two electrodes opening a gap of 1 volt.

5.2.2 Transmission Spectra

The total transmission spectrum $T(\epsilon, V)$ is plotted as function of the energy in Fig. 9a, b, c for applied voltage: V= 0, +1, +2 volt(s), respectively. We notice that the symmetry of the plots for the system without Si barrier is here completely destroyed by the presence of the barrier.

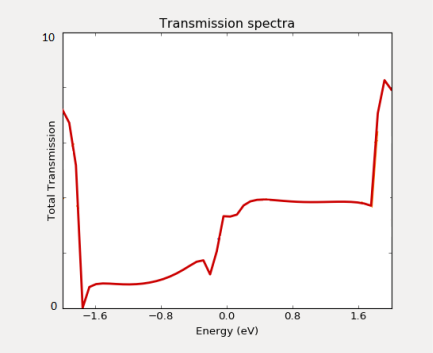

V=0

Figure 9a: Transmission spectra as function of the energy, decreases in all energy levels specially at $-1.6ev < \epsilon < 0ev$ in compare with perfect GNR

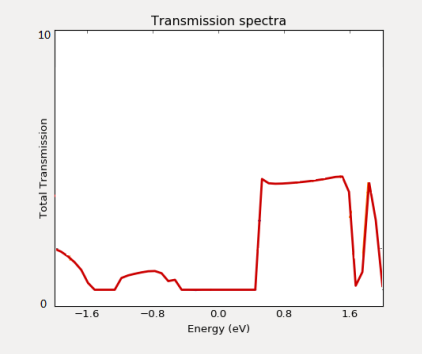

V=+1v

Figure 9b: Transmission spectra as function of the energy, decreases at $-1.6ev < \epsilon < -0.4ev$ in compare with perfect GNR at V=+1v

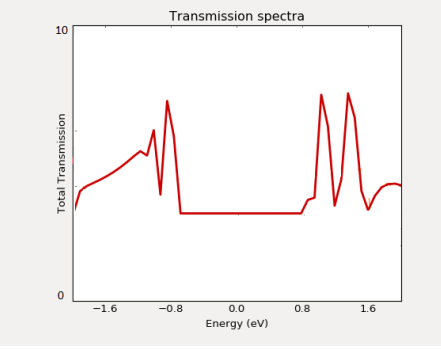

V=+2v

Figure 9c:Transmission spectra as function of the energy, decreases at $-2ev < \epsilon < -1.3ev$ in compare with perfect GNR at V=+2v

5.2.3 Spectral current

The spectral current is plotted in Fig. 10a, b, c for applied voltage: V= 0, +1, +2, volt(s), respectively.

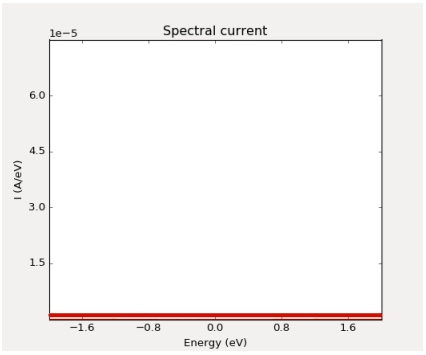

V=0

Figure 10a: No current spectral at V=0v

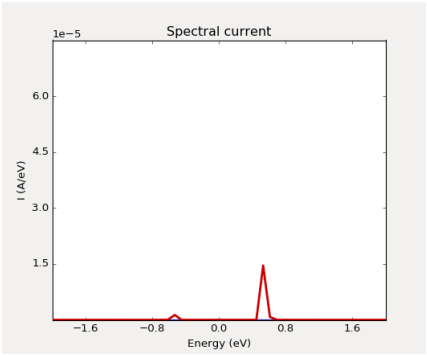

V=+1v

Figure 10b: Current spectral decreased completely in compare with perfect GNR at V=+1v

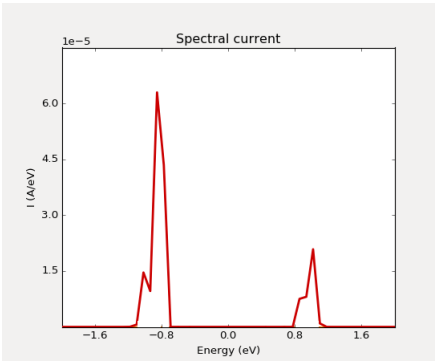

V=+2v

Figure 10c: Current spectral increased at $\epsilon = -1.2ev$ in compare with perfect GNR at V=+2v

What we can observe here is that Si atoms act as a barrier between the two electrodes opening a gap of 1 volt.

5.2.4 Transmission spectrum comparison

Fig 11 shows the total T(E) as function of energy.The transmission spectrum of perfect Graphene NanoRibbon is also added for comparison.
The average Fermi energy of the two electrodes is set to zero and V=0.

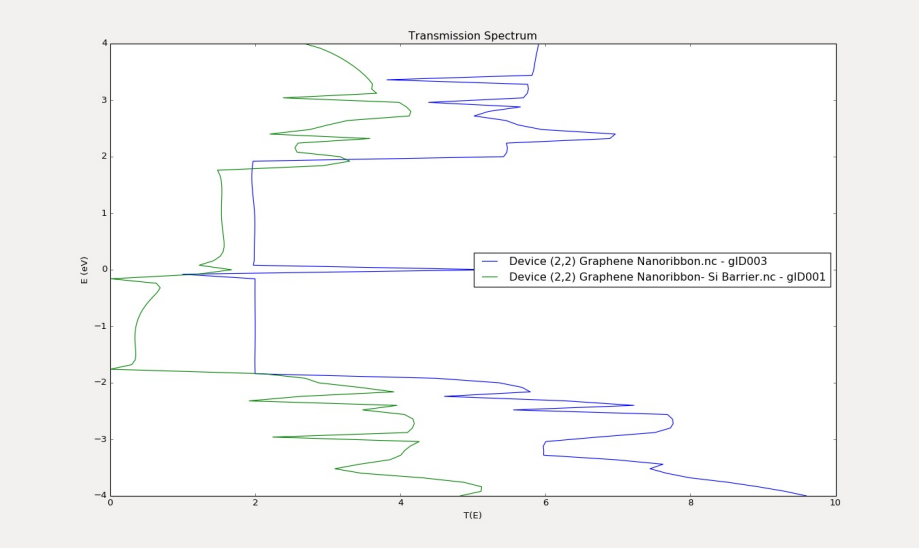

Figure 11: Transmission spectrum comparison of perfect GNR and GNR with Si barrier. Decreasing in all energy levels can be observed.

5.2.5 Transmission pathway

Transmission pathway shows how the electron propagates through a device at a specific energy value.
Fig 12 shows the transmission pathway through the device at $\epsilon = 0\,ev$ and V=0.

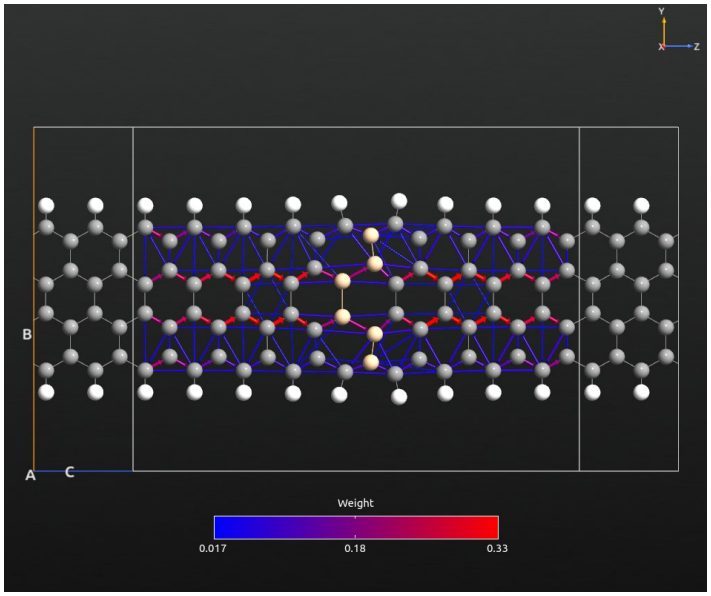

If compared with Fig. 6 we see that the most part of the low energy paths are concentrated in the extended regions of the NanoRibbon, while the high energy paths are in the central region.

5.3 Transmission Spectrum Comparison

Figure 13 shows a transmission spectrum comparison of perfect Graphene NanoRibbon with Graphene NanoRibbon with 3 Si and also with Graphene NanoRibbon with Si barrier.

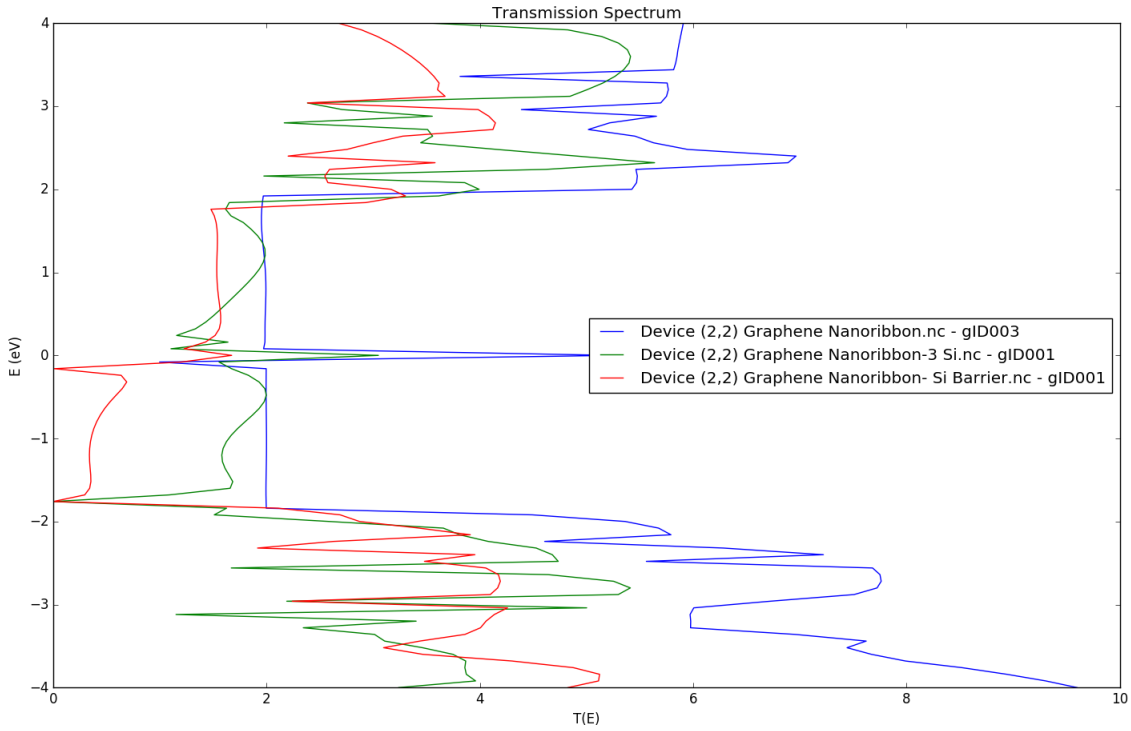

Figure 13

It can be observed that step by step as much as we substitute more Si atoms with C atoms in the Graphene NanoRibbon the total transmission spectrum decreased till it approximately getting near zero in the negative values of energy between 0 and -1.8 in the Graphene NanoRibbon with Si barrier.

5.4 I(V) Curve Comparison

Figure 14 shows the I(V) curve comparison of described systems.

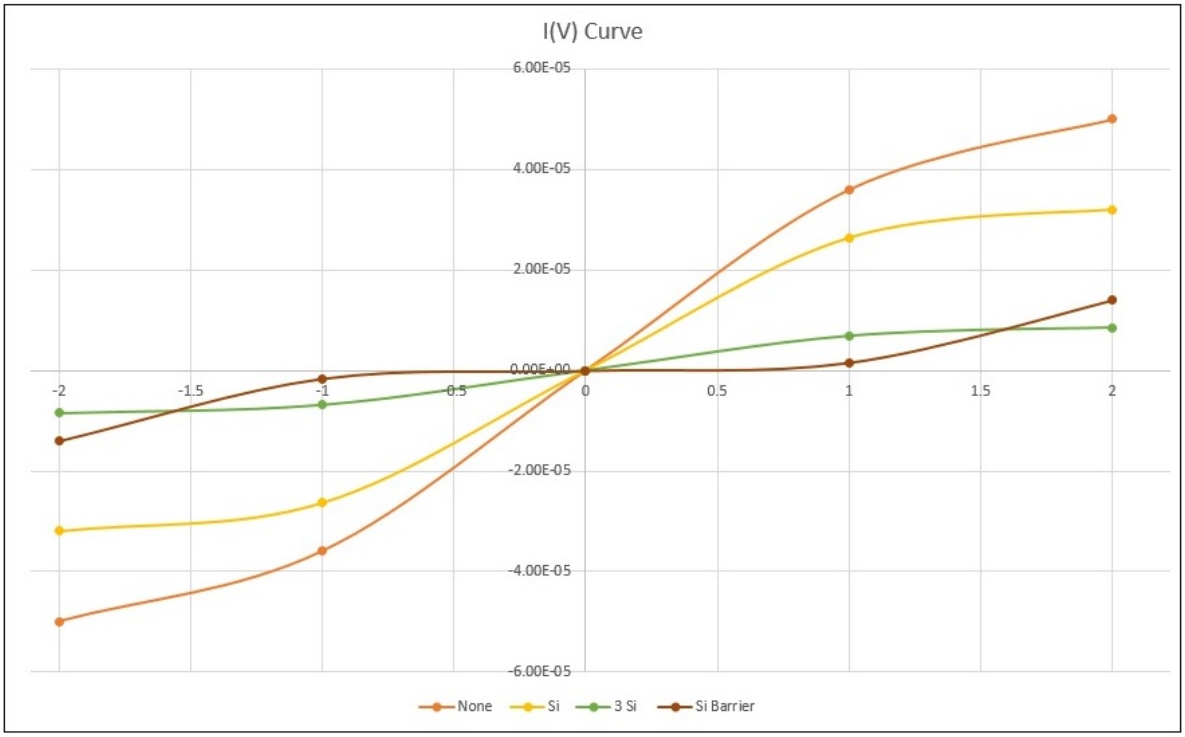

Figure 14

It can be observed that Si substitution with C atoms in Graphene NanoRibbon decreases the current via bias voltage, until formation of a barrier of Si atom that opens a gap, transforming the system into a semiconductor.

Chapter 6

6 MODEL SYSTEMS FOR PROTOTYPE CALCULATIONS

In this chapter, we consider devices with electrodes made of a material different from that of the "Conductor". In these examples, the material is Gold.

6.1 Au25-2*2 Graphene nanoribbon-Au25

The device consist of two electrodes, each one made up by 25 Au atoms, 25 Au atoms in the extension area, and by a 2*2 Zig-Zag Graphene NanoRibbon, sideways saturated by H atoms and connected to the gold electrodes as shown in Fig.1 and 2. The geometry of Graphene NanoRibbon has been optimized.

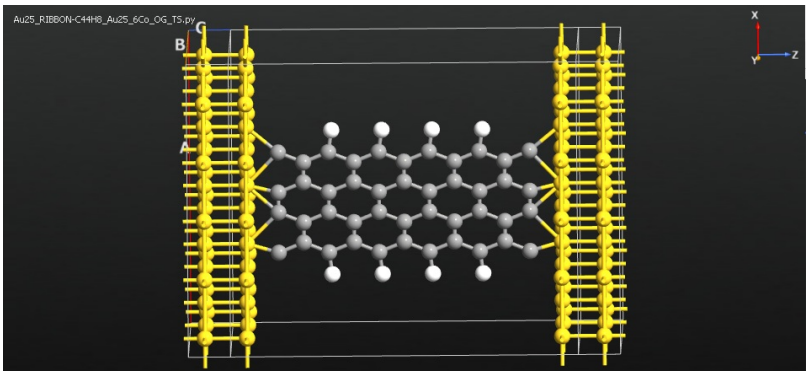

Figure 1: ZigZag Graphene NanoRibbon, saturated at the sides, between Gold electrodes

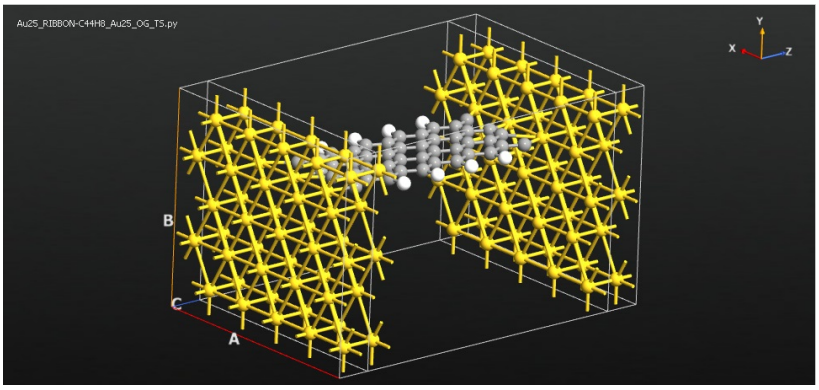

Figure 2: The same system, from different point of view

The central region has been relaxed by minimizing the energy of the structure with respect to the geometrical parameters on this device. We calculated the following quantities defined in details in the previous chapters [see also Ref 13],
1) Electronic current:

$$I(V) = \frac{2e^2}{h} \int_{-\infty}^{+\infty} d\epsilon [n_F(\epsilon - \mu_L) - n_F(\epsilon - \mu_R)] * T_r[\Gamma^\dagger \Gamma(\epsilon)] \tag{83}$$

2) Derivative of the electronic current:

$$\frac{dI(V)}{dV} \tag{84}$$

3) Left to right transmission amplitude matrix:

$$t(\epsilon) = [\Gamma_R(\epsilon)]^{1/2} G(\epsilon) \ [\Gamma_L(\epsilon)]^{1/2} = U_R \ diag\{|\ \tau_n\ |\} U_L^\dagger \tag{85}$$

defined in terms of its eigenvalues and eigenvectors.

6.1.1 I and dI/dV curves

The electronic current through the contacts: I(V), and its derivatives: dI/dV have been plotted, respectively in Fig 3a and 3b.
We see that I(V) is an anti symmetric function of the voltage: I(V)= -I(-V), while its derivative symmetric is: $\frac{dI}{dV}(V) = \frac{dI}{dV}(-V)$.

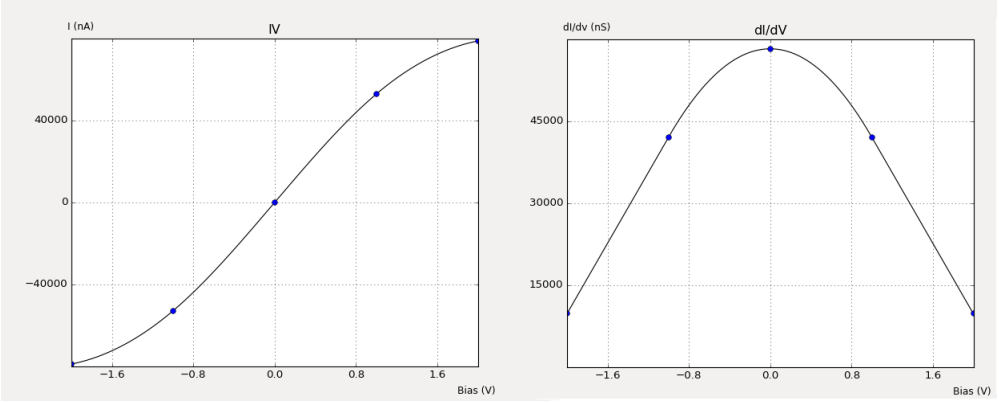

Figure 3a: I(V) curve of GNR with Gold electrodes

Figure 3b: dI/dV curve of GNR with Gold electrode

Comparison with the same plots for device with electrodes of Graphene shows a relevant increase of the current when gold electrodes are used.

6.1.2 Transmission Spectra

The total transmission spectrum $T(\epsilon) = \sum_n \mid \tau_n \mid^2$ is the sum of the eigenvalues of the transmission amplitude matrix [see Ref 13] and is plotted as function of the energy in Fig. 4a, b, c for applied voltage: V= 0, +1, +2 volt(s), respectively.

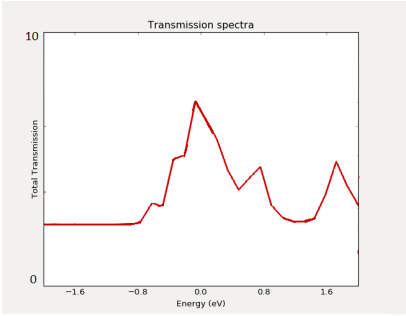

V=0

Figure 4a: Transmission spectra as function of the energy

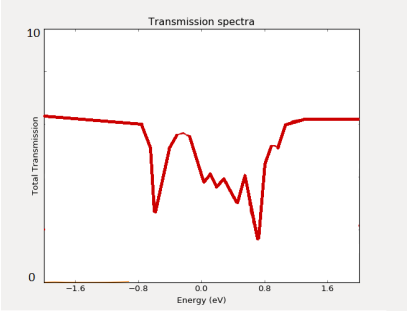

V=+1v

Figure 4b: Transmission spectra as function of the energy

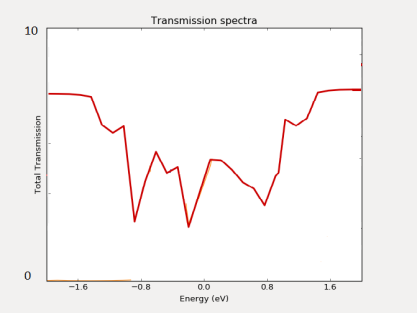

V=+2v

Figure 4c: Transmission spectra as function of the energy

Asymmetries and different shapes which can be observed in transmission spectra, when compares with, Graphene NanoRibbon on Graphene electrodes, are due to the interference of the central region(Graphene NanoRibbon) and electrodes(Golds).

6.1.3 Spectral current

The spectral current defined as the integral of the Landauer formula, is plotted in Fig. 5a, b, c for applied voltage: V= 0, +1, +2, volt(s), respectively.

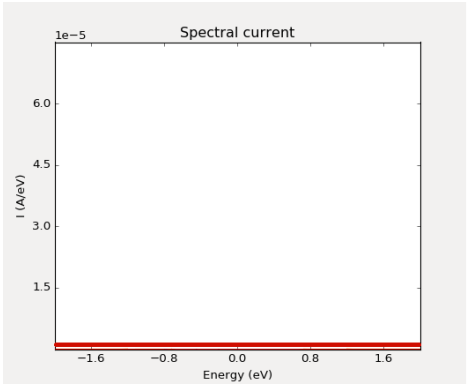

V=0

Figure 5a: No current spectral at V=0

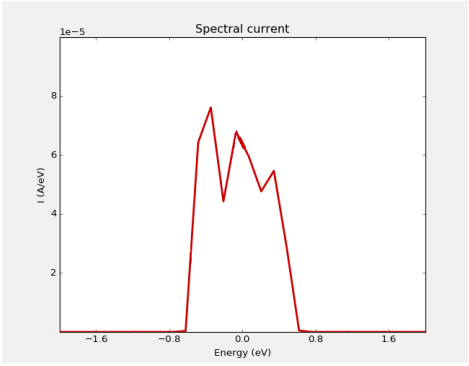

V=+1v

Figure 5b: Current spectral of GNR between Gold electrodes. Current only between $\pm 0.8ev$

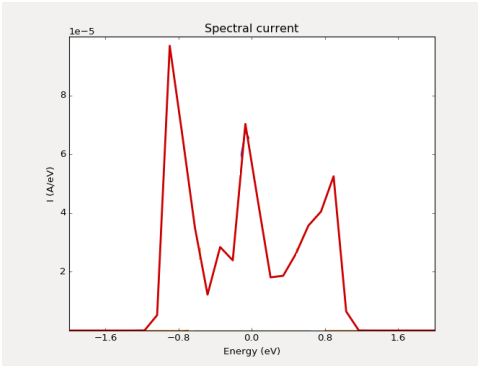

V=+2v

Figure 5c: Current spectral of GNR between Gold electrodes. Current only between $\pm 1.2ev$

Comparison with the same plots made for the same system between gold electrodes shows the vanishing of any symmetry in the plots.

6.1.4 Transmission pathways

Transmission pathway shows how electrons propagate through device at a specific energy value.
Fig 6 shows the transmission pathway through the device at $\epsilon = 0\,ev$ and V=0.

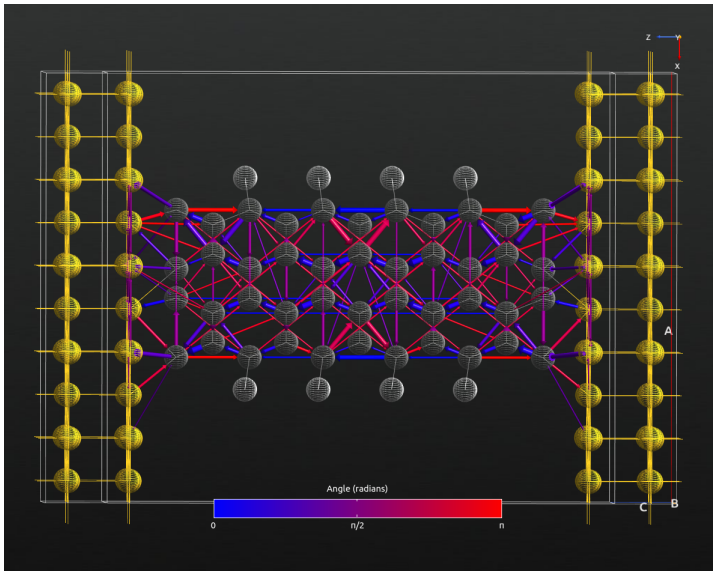

Figure 6: Transmission pathways at the Fermi level for the GNR with Gold electrodes

If compared with transmission pathways of Graphene NanoRibbon on Graphene electrodes, we notice asymmetries and different pathways due to the interference of the central region(Graphene NanoRibbon) and electrodes(Golds).

6.2 Au25-2*2 zig-zag Graphene nanoribbon on SiO_2-Au25

This system contains 25 Au atoms as an electrode for each left and right part of the device, plus 25 Au atoms as the extension area for each left and right side.
In the central region, there is a 2*2 zig-zag Graphene NanoRibbon, grown on a crystal substrate of $SiO2$. The system has been relaxed at fixed electrodes. We notice the presence of conductive channels with conjugated double bonds and channels made by single bonds. Graphene NanoRibbon is corrugate because of formation of C-O bonds connecting the Graphene NanoRibbon to the substrate.[see Ref 15]

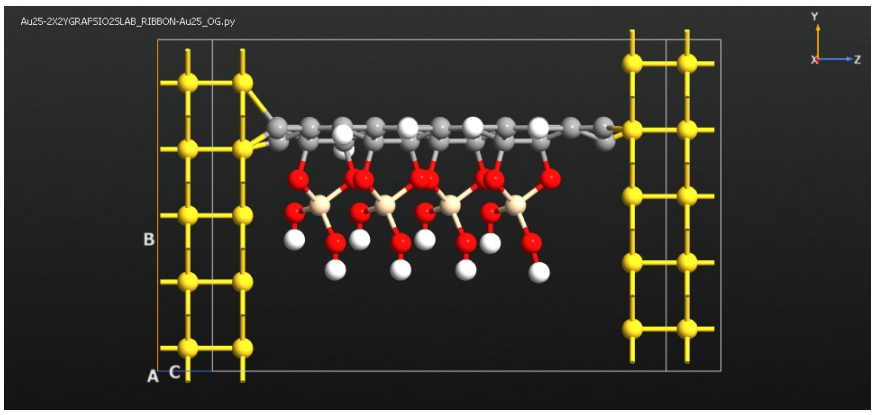

Figure 7: ZigZag Graphene NanoRibbon saturated at the sides grown on SiO_2 substrate, between Gold electrodes

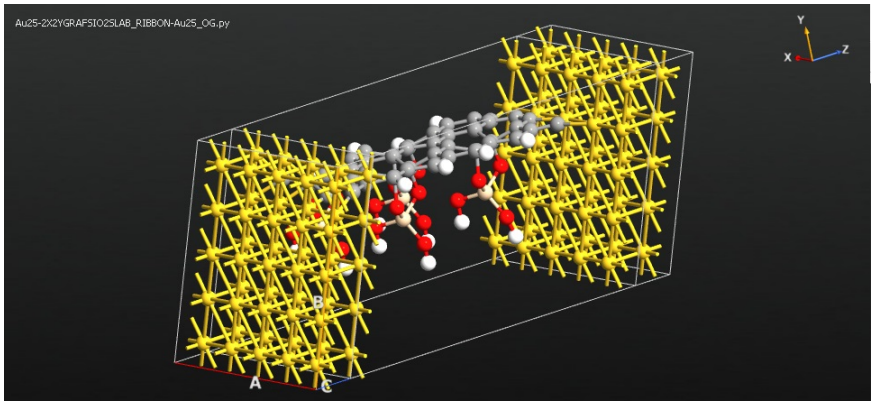

Figure 8: The same system from different point of view

6.2.1 I and dI/dV curves

The electronic current through the contacts: I(V), and its derivatives: dI/dV have been plotted, respectively in Fig 9a and 9b.

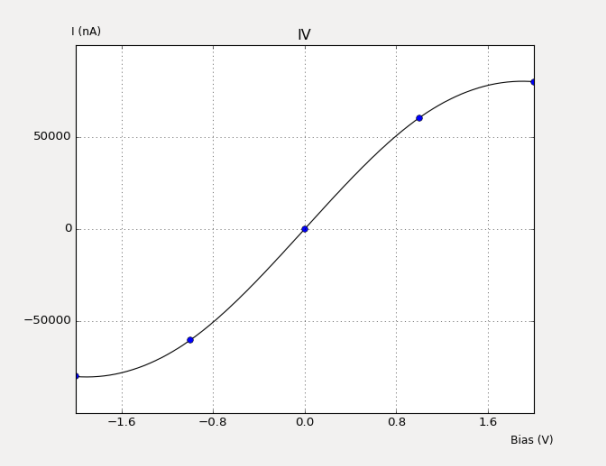

Figure 9a: I(V) curve of GNR grown on SiO_2 substrate, with Gold electrodes. Increasing in current can be observed in compare with GNR between Gold electrodes.

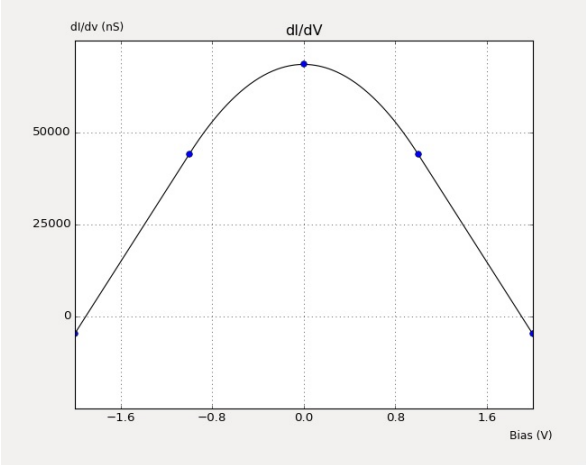

Figure 9b: dI/dv curve of GNR grown on SiO_2 substrate, with Gold electrodes

We notice an increase of the current as compare to I(V) plots calculated for the Graphene NanoRibbon between gold electrodes of Fig. 1,2.

6.2.2 Transmission Spectra

The total transmission spectrum $T(\epsilon, V)$ is plotted as function of the energy in Fig.10 a, b, c for applied voltage: V= 0, +1, +2 volt(s), respectively.

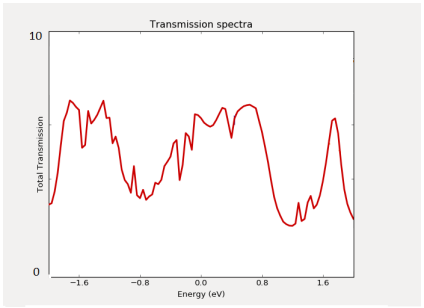

V=0

Figure 10a: Transmission Spectra of GNR grown on SiO_2 substrate between Gold electrodes.

Increasing in all energy levels can be observed specially at $-2ev < \epsilon < -0.8ev$ in compare with GNR between Gold electrodes.

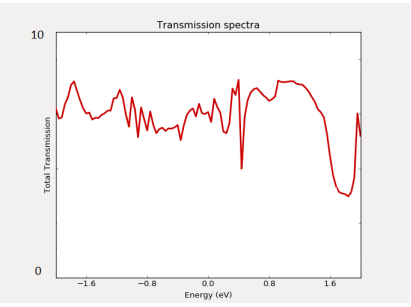

V=+1v

Figure 10b: Transmission Spectra of GNR grown on SiO_2 substrate between Gold electrodes.

Increasing in all energy levels can be observed specially at $-0.8ev < \epsilon < 0.8ev$ in compare with GNR between Gold electrodes.

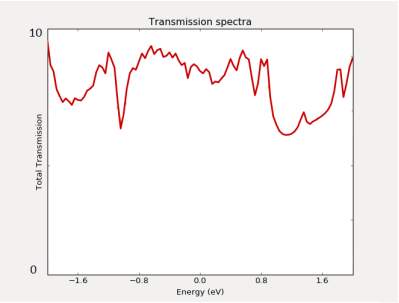

V=+2v

Figure 10c: Transmission Spectra of GNR grown on SiO_2 substrate between Gold electrodes.

Increasing in all energy levels can be observed specially at $-1.2ev < \epsilon < -1.2ev$ in compare with GNR between Gold electrodes.

6.2.3 Spectral current

The spectral current is plotted in Fig. 11 a, b, c for applied voltage: V= 0, +1, +2, volt(s), respectively.

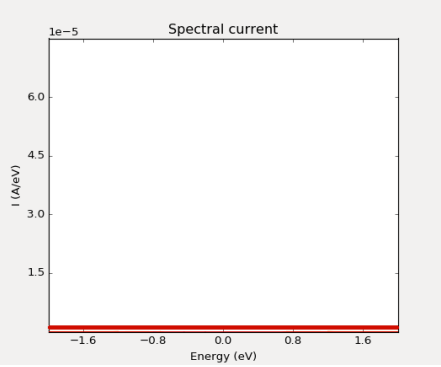

V=0

Figure 11a: No current spectral at V=0

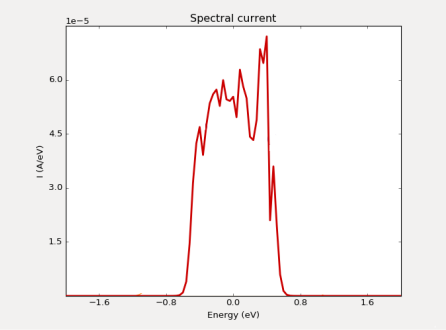

V=+1v

Figure 11b: Current Spectral of GNR grown on SiO_2 substrate between Gold electrodes.

Current spectral increases at $-0.7ev < \epsilon < 0.7ev$ in compare with GNR with Gold electrodes at V=+1v

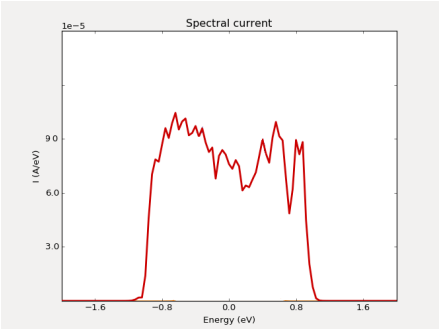

V=+2v

Figure 11c: Current Spectral of GNR grown on SiO_2 substrate between Gold electrodes.

Current spectral increases at $-1.2ev < \epsilon < 1.2ev$ in compare with GNR with gold electrodes at V=+2v

Chapter 7

7 Nano Scale FET Transistor

A Field Effect Transistor consists of a gate, a channel region connecting source and drain electrodes, and a barrier separating the gate from the channel (Fig. 1). The operation of a conventional FET relies on the control of the channel conductivity, and thus the drain current, by a voltage, V_{GS}, applied between the gate and source.

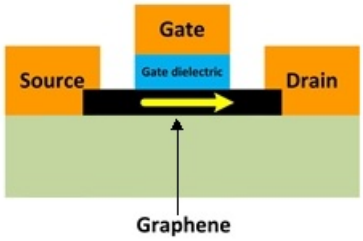

Fig. 1: Schematic view of field effect transistor with Graphene NanoRibbon as a channel

The possibility of having channels that are just one atomic layer thick is perhaps the most attractive feature of graphene for use in transistors. Single-layer graphene is a purely two-dimensional material. Its lattice consists of regular hexagons with a carbon atom at each corner. The bond length between adjacent carbon atoms, is $1.42A°$. The most frequently stated advantage of graphene is its high carrier mobility at room temperature. The conductivity, stability, uniformity, composition, and 2D nature of graphene make it an excellent material for electronic devices.

7.1 GFET

A Graphene Field Effect Transistor (GFET) is composed of a graphene channel between two electrodes with a gate contact to modulate the electronic response of the channel. SiO_2, Al_2O_3, and HfO_2 can be used as a dielectric between the channel and the gate.

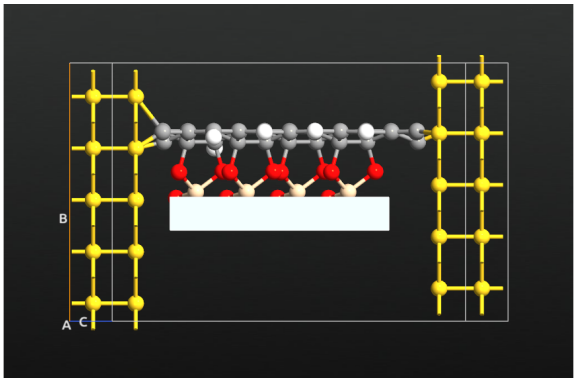

Fig. 2: Graphene NanoRibbon Field Effect Transistor,with Golden Source and Drain contact and SiO_2 as a gate dielectric

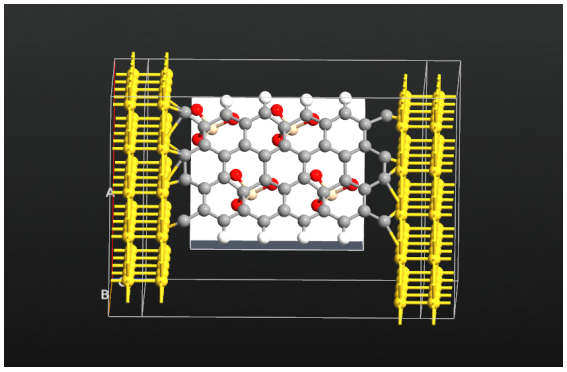

Fig. 3: The same system with different point of view

The simulated structure is presented in Fig.2,3: the device presents a single gate topology with very thin oxide layer (silicon oxide thickness t_{ox} has been set to $4.2A°$), in order to maximize the electrostatic control over the channel. The symmetric $10A°$- long source and drain regions have been n-doped, while the channel has been p-doped. The doping concentration for source and drain regions has been fixed at $4*10^{19}e/cm^3$ and $0.001337e/atom$ for the channel.V_{DS} set to $0.5v$. Gate length and width set to $10.6A°$ and $1.6A°$, respectively.

7.1.1 Transmission Spectrum

The transmission spectrum for V_G as a function of the energy, where $-1v < V_G < 5v$ have been studied and shown in Fig. 4 to 10.

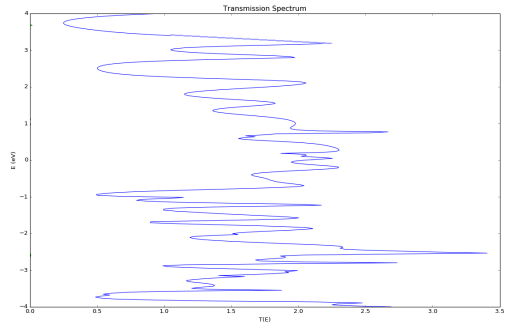

V_G= -1v

Fig. 4: Transmission spectrum as function of the energy at $V_{SD} = 0.5v$ and $V_G = -1v$

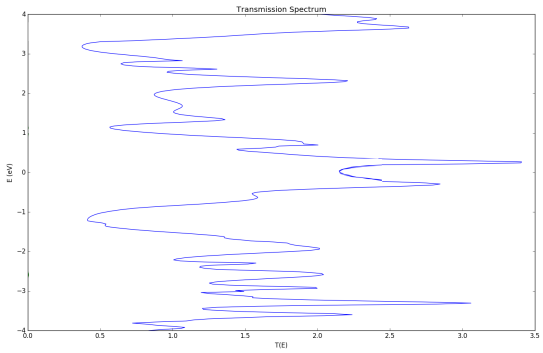

V_G= 0v

Fig. 5: Transmission spectrum as function of the energy at $V_{SD} = 0.5v$ and $V_G = 0v$

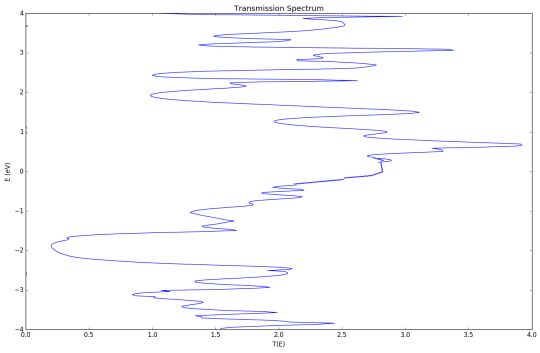

V_G= +1v

Fig. 6: Transmission spectrum as function of the energy at $V_{SD} = 0.5v$ and $V_G = +1v$

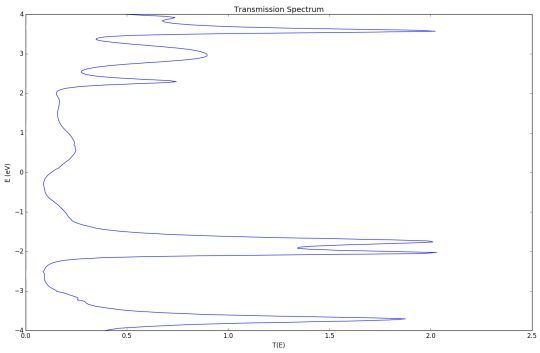

V_G= +2v

Fig. 7: Transmission spectrum as function of the energy at $V_{SD} = 0.5v$ and $V_G = +2v$, decreasing in transmission spectrum can be observed.

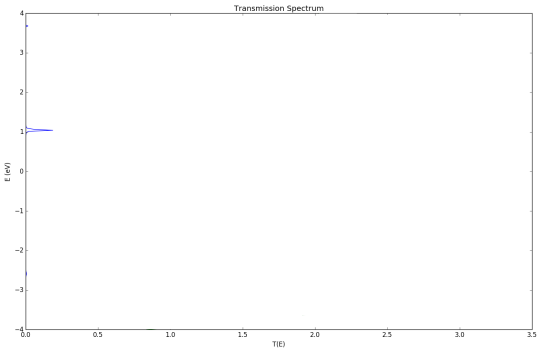

V_G= +3v

Fig. 8: Transmission spectrum as function of the energy at $V_{SD} = 0.5v$ and $V_G = +3v$, transmission spectrum completely decreased and getting near zero at $V_G = +3v$

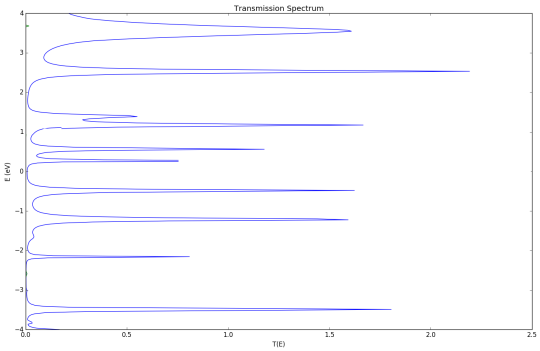

V_G= +4v

Fig. 9: Transmission spectrum as function of the energy at $V_{SD} = 0.5v$ and $V_G = +4v$, increasing in transmission spectrum can be observed

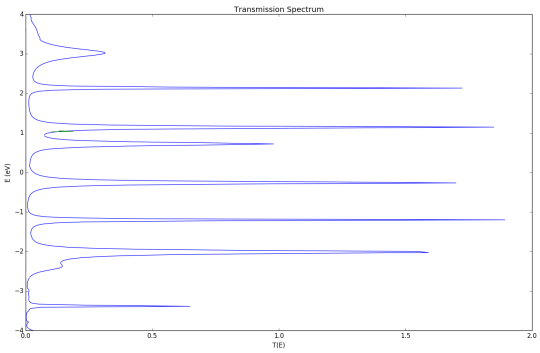

V_G= +5v

Fig. 10: Transmission spectrum as function of the energy at $V_{SD} = 0.5v$ and $V_G = +5v$

It can be observed that changing the gate voltage can affect the transmission properties of graphene nanoribbon which at $V_G = 3v$ it completely stop the transmission through the channel.

7.1.2 Channel Conductance

Channel conductance via different gate voltage has been plotted.

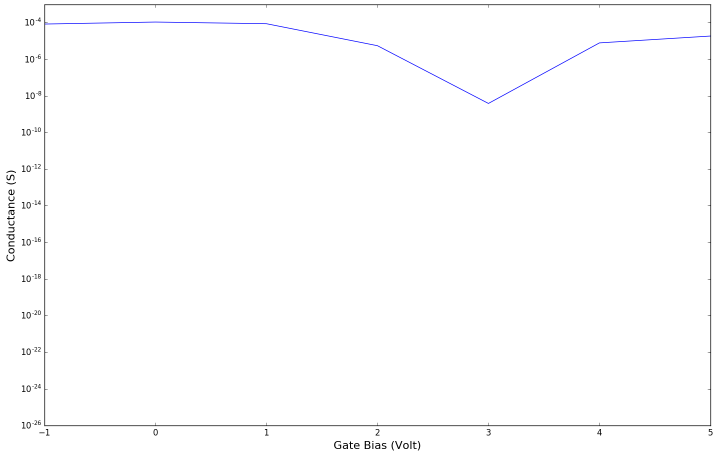

Fig. 11: Channel conductance via gate bias voltage. At $V_G = +3v$ the channel has the least conductance. I_{On}/I_{Off} ratio is about 10^4

It shows the channel conductance via gate voltage(V_G). I_{On} to I_{Off} ratio is about 10^4 which is acceptable for FET transistors.

7.2 GFET with Si Barrier

The simulated structure is presented in Fig.11 and 12. The device presents a single gate topology with very thin oxide layer, in order to maximize the electrostatic control over the channel. All the properties has been set the same as previous device except 6 C atoms substituted by 6 Si atoms to work as a barrier. This device has much more larger band gap, we expect a better properties.

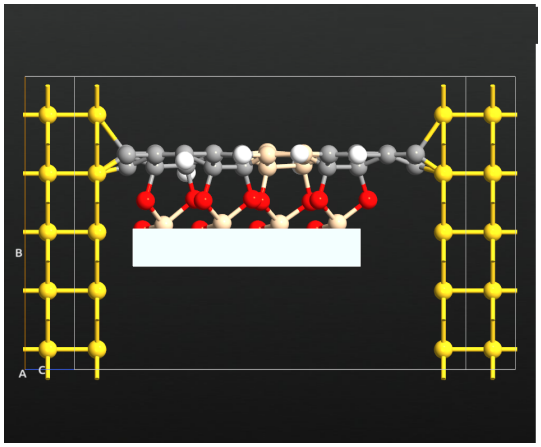

Fig. 12: Graphene NanoRibbon Field Effect Transistor with Golden Source and Drain contact and SiO_2 as a gate dielectric, with one layer of Si Barrier in the channel region

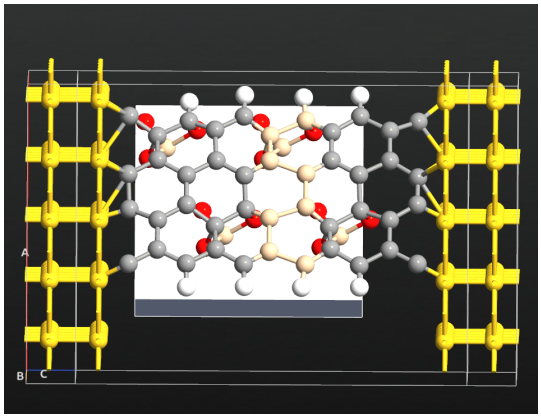

Fig.13: The same system with different point of view.

7.2.1 Transmission Spectrum

The transmission spectrum for different V_Gs as a function of the energy, where $-1v < V_G < 5v$ have been studied and shown in Fig 14.

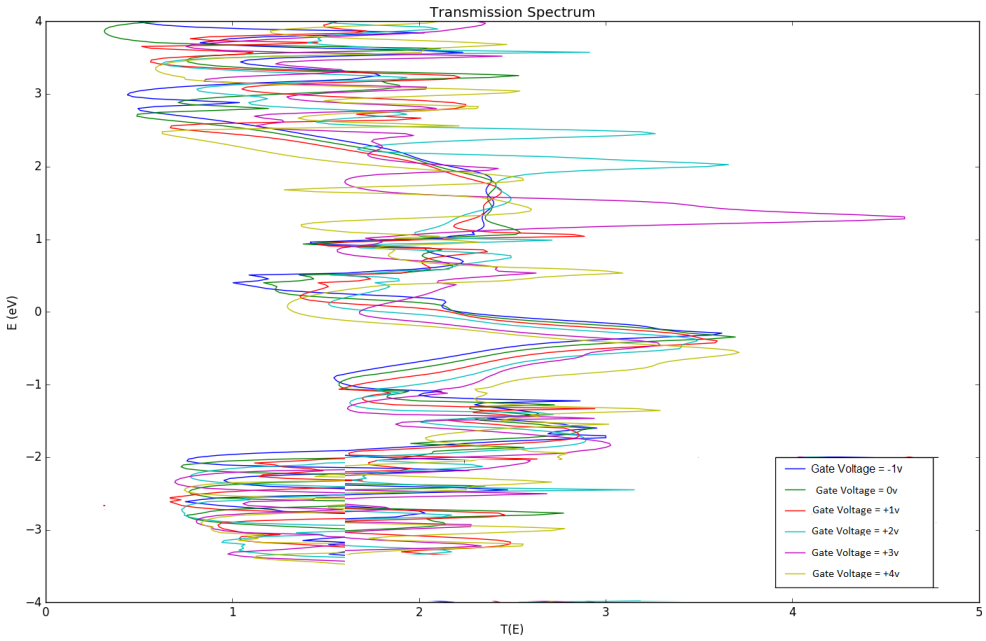

Fig. 14: Transmission spectrum as function of the energy at $V_{SD} = 0.5v$ and $-1v < V_G < +5v$, approximately similar transmission spectrum for different gate bias voltage can be observed due to a quantum tunneling effect.

It can be observed that changing the gate voltage could not affect the transmission properties as we expected, although its larger band gap. The results can be explained due to quantum tunneling effect through the barrier. It can also be observed that quantum tunneling effect has a very poor dependency on the gate voltage.

7.2.2 Channel Conductance

The channel conductance via gate bias voltage has been plotted in Fig.15. It shows a poor dependency of conductance to gate bias voltage, which is approximately constant.

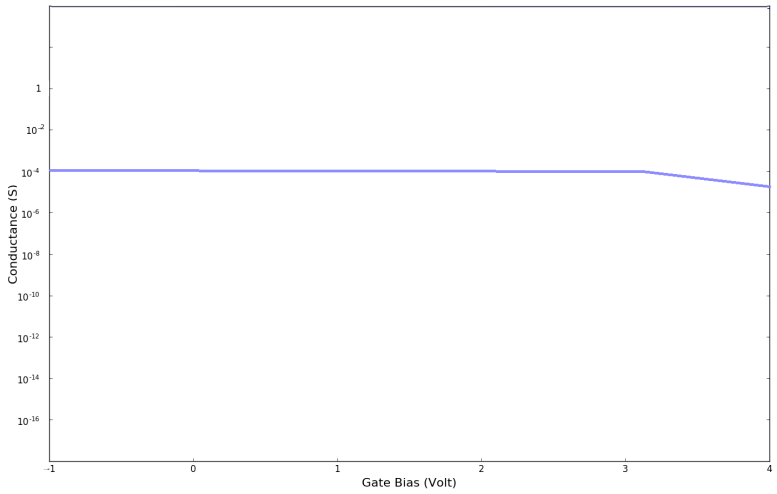

Fig. 15: Channel conductance via gate bias voltage. Channel conductance does not change via changing the gate bias voltage and it's approximately constant.

7.3 GFET with BN barrier

The simulated structure is presented in Fig.15 and 16. Graphene nanoribbon grown on SiO_2 which 3 C layers substituted with BN layers. BN with a honeycomb structure has less impact and most similarity with graphene nanoribbon. The device presents a single gate topology with very thin dielectric layer, in order to maximize the electrostatic control over the channel.footnotesize [see Ref 16, 17]

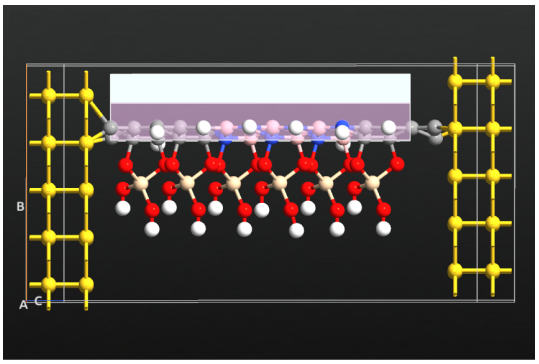

Fig. 16: Graphene NanoRibbon field effect transistor with Golden Source and Drain contact and 3 layer of BN barrier in channel region

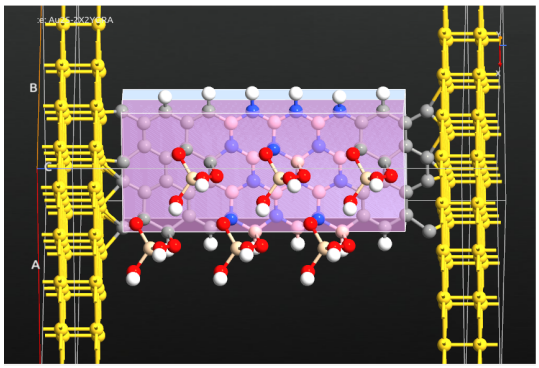

Fig.17: The same system from different point of view.

7.3.1 Transmission Spectrum

The transmission spectrum for V_G as a function of the energy, where$-1 < V_G < 5$ have been studied and shown in Fig 18 to 24.

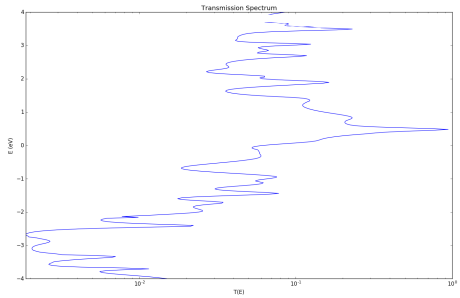

V_G= -1v

Fig. 18: Transmission spectrum as function of the energy at $V_{SD} = 0.6v$ and $V_G = -1v$

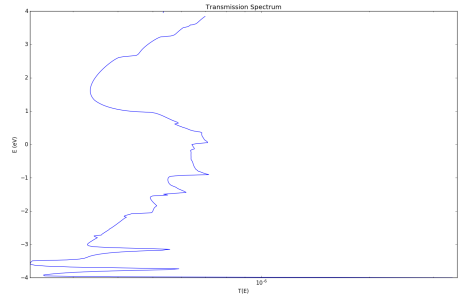

V_G= 0v

Fig. 19: Transmission spectrum as function of the energy at $V_{SD} = 0.5v$ and $V_G = 0v$, decreasing in transmission spectrum can be observed
(Pay attention to the T(E) dimension)

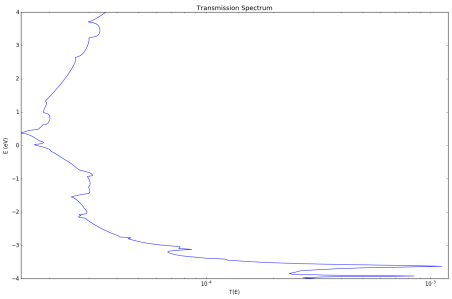

V_G= +1v

Fig. 20: Transmission spectrum as function of the energy at $V_{SD} = 0.5v$ and $V_G = +1v$, increasing in transmission spectrum can be observed
(Pay attention to the T(E) dimension)

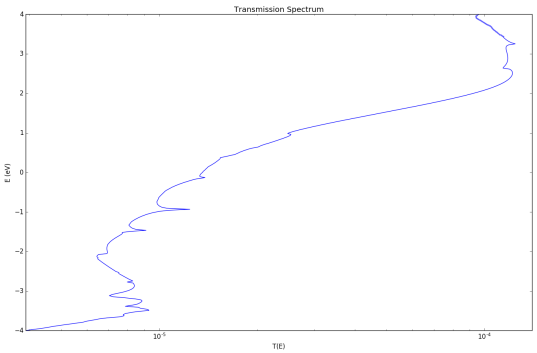

V_G= +2v

Fig. 21: Transmission spectrum as function of the energy at $V_{SD} = 0.5v$ and $V_G = +2v$ (Pay attention to the T(E) dimension)

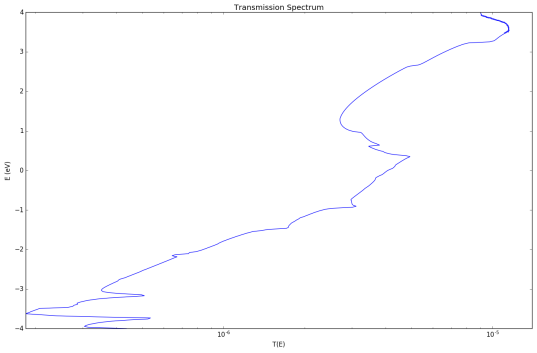

V_G= +3v

Fig. 22: Transmission spectrum as function of the energy at $V_{SD} = 0.5v$ and $V_G = +3v$ (Pay attention to the T(E) dimension)

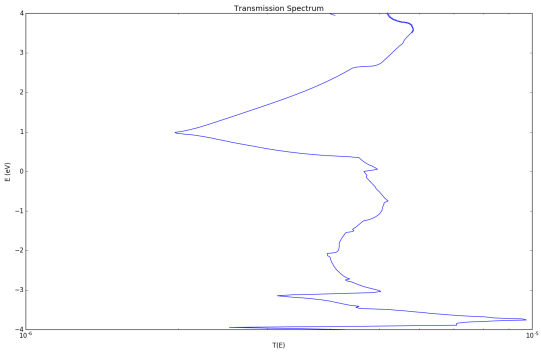

V_G= +4v

Fig. 23: Transmission spectrum as function of the energy at $V_{SD} = 0.5v$ and $V_G = +4v$ (Pay attention to the T(E) dimension)

It can be observed that changing the gate voltage can affect the transmission properties of channel which at $V_G = 0v$, it completely stop the transmission through the channel.

7.3.2 Channel Conductance

Channel conductance via gate bias voltage has been plotted in Fig. 25.

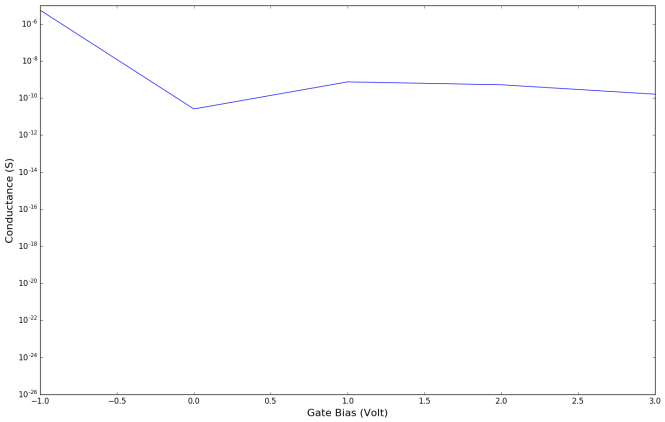

Fig. 25: Channel conductance via gate bias voltage. At $V_G = 0v$ the channel has the least conductance. I_{On}/I_{Off} ratio is about 10^5

It shows the channel conductance via gate bias voltage(V_G). I_{On} to I_{Off} ratio is about 10^5 which is so much better than Graphene NanoRibbon FET.

In this chapter we have provided an accurate investigation of the transmission properties of ZigZag Graphene NanoRibbon grown on SiO_2 substrate with golden source and drain, as a FET. We also try to implement a barrier to open a band gap for Graphene NanoRibbon; to study how opening a band gap can affect its properties.
In single layer barrier structure, we have found the tunneling effect. Our results show that tunneling effect is only slightly depend on energy in the band gap.
In 3 layers barrier structure, obtained by substituting Boron Nitrite with Graphene layers, we have shown that tunneling does not occur. We observe an increase in I_{On}/I_{Off} ratio in compare with Graphene NanoRibbon FET. Further study is required to better understand transmission properties of FETs in case in which hetrostructures are not lattice-matched.

Bibliography

[1] Physical Chemistry Chemical Physics(PCCP) journal –http://pubs.rsc.org/

[2] G. Binnig, H. Rohrer, C. Gerber, and E. Weibel, Phys. Rev. Lett. 49(1), 5761 (1982).

[3] G. Binnig, C. F. Quate, and C. Gerber, Phys. Rev. Lett. 56(9), 930933 (1986).

[4] A. Aviram and M. A. Ratner, Chem. Phys. Lett. 29, 277 (1974).

[5] Jiang,L.;Yuan,L.,C.A.Controlling Leakage Currents, 2014, 136, 19821991.

[6] Forty years of molecular electronics: Non-equilibrium heat and charge transport at the nanoscale-Justin P. Bergeld and Mark A. Ratner (2013).

[7] A. J. Kronemeijer,Functional Molecular Electronics, PhD Thesis, Rijksuniversiteit Groningen, (2011)

[8] M. Paulsson, F. Zahid, and S. Datta. Nanoscience, Engineering and Technology Handbook, chapter Resistance of a Molecule. CRC Press, 2002. Editors, D. Brenner, S. Lyshevski and G. Iafrate, condmat/0208183.

[9] P. S. Damle, A. W. Ghosh, and S. Datta. Molecular nanoelectronics, chapter Theory of nanoscale device modeling. 2002. Editor M. Reed.

[10] F. Zahid, M. Paulsson, and S. Datta. Advanced Semiconductors and Organic Nano-Techniques, chapter Electrical Conduction through Molecules. Academic press, 2002. Editor H. Markoc.

[11] S. Datta. Electronic transport in mesoscopic systems. Cambridge University Press, Cambridge, UK, 1997.

[12] L. E. Ballentine. Quantum mechanics. World Scientic, 1998. see chapter 16, Scattering.

[13] PRB 65, 165401(2002)

[14] ATK Manual, Section ATK-DFT, Section NEGF formalism

http://docs.quantumwise.com/manual

[15] Phys. states solid B253, No9, 1799 - 1807(2016) R. Colle *et al*

[16] G. Fiori, A. Betti. Lateral Graphene hBCN Hetrostructures as a platform for fully 2D transistors, ACSNANO, 2012

[17] S. Bruzzone, D. Logoteta. Vertical transport in graphene hexagonal boron nitride heterostructure devices. Scientific Reports, 2015

[18] Atomistix ToolKit version 2016.3, QuantumWise A/S (www.quantumwise.com)

[19] Virtual NanoLab version 2016.3, QuantumWise A/S (www.quantumwise.com)

[20] M. Brandbyge, J.-L. Mozos, P. Ordejn, J.
Taylor, and K. Stokbro, Phys. Rev. B 65, 165401 (2002).

[21] J. M. Soler, E. Artacho, J. D. Gale, A. Garca, J. Junquera, P. Ordejn, and D. Snchez-Portal, J. Phys. Condens. Matter 14, 2745 (2002).